Table 3. Clinical Characteristics

	Total (n=45)	Group A (n=21)	Group B (n=24)	*P* Value
Proband, n, (%)	21	12 (57)	9 (38)	0.230
Age at diagnosis, average, y, ±SD	23±16	20±14	26±16	0.142
Female, n (%)	27 (60)	12 (57)	15 (63)	0.684
Baseline ECG				
HR, average, ms, ±SD	76±22	75±19	77±25	0.565
QTc, average, ms, ±SD	430±42	418±42	440±40	0.285
QUc, average, ms, ±SD	667±50	695±52	643±35	0.004*
T amp, average, mV, ±SD	0.51±0.27	0.56±0.28	0.46±0.26	0.215
U amp, average, mV, ±SD	0.21±0.08	0.24±0.07	0.18±0.08	0.024*
Tp-Up, average, ms, ±SD	214±31	224±32	204±28	0.151
U/T ratio, average, ±SD	0.57±0.5	0.66±0.66	0.48±0.3	0.601
Arrhythmias, patients, n (%)				
PVC	30 (67)	19 (90)	11 (46)	0.032*
Bidirectional VT	15 (33)	10 (48)	5 (11)	0.195
Polymorphic VT	5 (11)	3 (14)	2 (8)	0.368
VF	1 (2)	0	1 (4)	0.571
Cardiac events				
Syncope, patients, n (%)	4 (9)	2 (10)	2 (8)	0.891
ACA, patients, n (%)	2 (4)	0	2 (8)	0.278
Treatment				
β-blockers	11 (24)	6 (29)	5 (21)	0.589
Flecainide	2 (4)	1 (5)	1 (4)	0.924
Verapamil	2 (4)	1 (5)	1 (4)	0.925
ICD implantation	1 (2)	0	1 (4)	0.533
Mutation site				
C-terminal, patients, n (%)	27 (60)	18 (85)	9 (38)	0.002*
Pore, patients, n (%)	2 (4)	1 (5)	1 (4)	0.925
N-terminal, patients, n (%)	16 (36)	2 (10)	14 (58)	0.001*

ACA indicates aborted cardiac arrest; ICD, implantable cardioverter-defibrillator; VT, ventricular tachycardia; VF, ventricular fibrillation.

Group A: *KCNJ2* mutation carriers showing ≥2 ATS features; group B: those showing only 1 of the ATS features or catecholaminergic polymorphic ventricular tachycardia; *$P<0.05$ compared with group A.

to group A (open sections in the pie chart of Figure 3). Six of them (13%) had all 3 features, 7 (16%) both (A) and (P), 7 (16%) both (A) and (D), and 2 (5%) both (D) and (P). On the other hand, 24 patients (53%) with 1 of the ATS features belonged to group B (closed sections of Figure 3): 11 (24%) only (A), 3 (9%) only (P), 2 (4%) only (D). Eight genotype-positive family members (18%) displayed only (U).

CPVT Phenotype in *KCNJ2* Mutation Carriers

We identified 2 *KCNJ2* mutations, G144D (Table 2, case 23) and T305S (case 24), in 2 of 28 probands with CPVT phenotypes (Table 1), without dysmorphic features or periodic paralysis. These 2 cases experienced first syncope after the age of 30 (G144D, 36 years old; T305S, 32 years old). Furthermore, these probands' ECGs showed bidirectional VT at rest as well, and, as in CPVT, exercise-aggravated ventricular arrhythmia. In the G144D case, ECG always showed a PVC bigeminy even at rest, and the exercise stress test increased PVC and produced polymorphic VTs. Flecainide (150 mg per day) reduced her VTs. In the T305S case, exercise also increased numbers of PVC. She had pVT and VF while nursing her son. Her baseline ECG showed no abnormal U waves (QUc=644 ms, Tpeak-Upeak interval=185 ms).

Comparison of Patients With Typical Versus Atypical Phenotype

Table 3 summarizes the clinical characteristics of patients and compares them between groups A and B. There were no significant differences in the number of probands, age at diagnosis, and sex. Group A had a significantly longer QUc interval (group A, 695±52 ms versus group B, 643±35 ms, $P=0.004$) and higher U wave (0.24 versus 0.18 mV, $P=0.024$). PVCs were significantly more frequent in group A (n=19 patients versus n=11 patients, $P=0.032$); however, the incidences of bVT, pVT, and ventricular fibrillation were not different between the 2 groups. There were also no

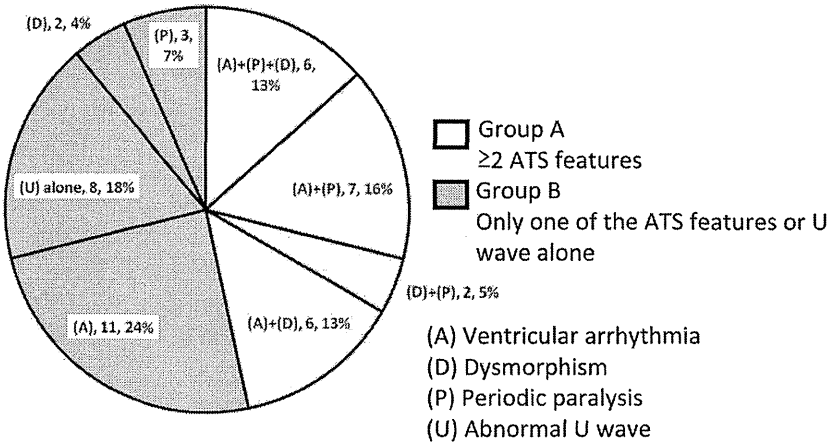

Figure 3. Prevalence of 3 features of Andersen-Tawil syndrome (ATS) among 45 *KCNJ2* mutation carriers (21 probands and 24 family members). (A) indicates ventricular arrhythmia; (P), periodic paralysis; (D), dysmorphic features; (U), abnormal U wave. **Open sections** indicate group A: patients who had ≥2 ATS features (n=21, 47%). **Closed sections** indicate group B (n=24, 53%): those who had only 1 of the ATS features or an abnormal U wave alone.

significant differences regarding the incidence of cardiac events and content of treatment.

Concerning the mutation site, C-terminal mutation carriers were more frequent in group A (n=18 versus n=9, P=0.002). In contrast, N-terminal mutations were more frequent in group B (n=2 versus n=13, P=0.001). As described above, we excluded 1 case with *KCNJ2* double mutations (Table 2, case 15) from this analysis. However his father, carrying a C-terminal mutation alone (V302 M), belonged to group A and showed a full set of ATS features. In contrast, his mother, carrying an N-terminal mutation (R80C), only displayed an abnormal U wave.

Functional Assay of 4 Mutants Found in Atypical Phenotype Group B

We conducted electrophysiological functional assays for 4 mutations in Group B—R82W, R82Q, G144D, and T305S (see Table 2; cases 16, 17, 23, and 24). Figure 4 A-a shows a family of current traces recorded from a CHO cell transfected with WT-KCNJ2 (1 μg). The lower inset in Figure 4A-a indicates the test pulse protocol. WT-*KCNJ2* expressed ample and time-independent currents showing a strong inward rectification, as depicted in the voltage-current relation in Figure 4B (closed squares). In contrast, all mutants (1 μg) were nonfunctional when expressed alone (Figure 4A-b). To simulate the allelic heterozygosity, WT and each of the mutant-*KCNJ2* clones were cotransfected at an equimolar ratio (0.5 μg each). Representative results are shown in Figure 4A-c. Outward *KCNJ2* channel currents were dominantly suppressed. In contrast, inward currents were variously reduced when coexpressed with WT.

From the results of multiple experiments, the mean current densities were measured at their respective test potentials. In Figure 4B, they are plotted as a function of the potentials, and in Figure 4C, those at −140 and −50 mV are presented as dot plots. Outward current densities at −50 mV when coexpressed with WT-KCNJ2 were 3.5±1.7 pA/pF in R82Q, 2.3±2.4 pA/pF in R82W, 2.6±0.9 pA/pF in G144D, and 8.1±2.4 pA/pF in T305S. Compared with the current densities obtained with the WT clone alone (1 μg, left plot in Figure 4C), the percent reductions were 95%, 97%, 96%, and 89%, respectively. In contrast, inward current densities at −140 mV were −162±20 pA/pF in R82Q, −152±22 pA/pF R82W, −43±13 pA/pF in G144D, and −199±20 pA/pF in T305S. Percent reductions were 58%, 39%, 89%, and 49%, respectively. Thus, G144D mutation exerted dominant negative suppression effects on both outward and inward currents. The other 3 mutations, however, had such effects only on outward currents.

Immunocytochemistry of Mutant Channels (R82Q, R82W, G144D, and T305S)

Regarding several *KCNJ2* mutations, impaired intracellular transport has been reported to cause loss of function. We therefore examined the trafficking of these 4 mutants and WT channels using an HA-tagging method. Figure 5 depicts typical results of confocal imaging. WT and HA-R82Q, HA-R82W, and HA-T305S mutants showed normal trafficking, whereas the HA-G144D mutant displayed no rim of red fluorescence, suggesting the presence of a trafficking defect.

Discussion

Prevalence of *KCNJ2* Mutation and ATS Features in Typical ATS

In the present study, we could identify heterozygous *KCNJ2* mutations in 24 (42%) of 57 probands of different cohorts showing typical ATS, and atypical phenotypes (1 of the ATS features or CPVT). Regarding 20 typical ATS (≥2 of 3 ATS features) probands, *KCNJ2* mutations were positive in 15 (75%). This value was comparable to those of previous reports: Plaster et al[4] identified 13 *KCNJ2* positives in 16 unrelated ATS kindreds (81%). Tristani-Firouzi et al[12] identified 17 *KCNJ2* positives in 25 kindreds (68%), and Donaldson et al[26] reported 9 positives in 17 kindreds (53%). The prevalence of *KCNJ2*-positive probands was, however, lower when screened in the total patients, compatible with long-QT syndrome (LQTS): Eckhardt et al[27] reported 4 *KCNJ2* mutation positives from 541 LQTS probands (0.74%). Fodstad et al reported 2 carriers in 188 LQTS patients (1%).[28]

Atypical ATS Phenotype

After excluding the compound mutation cases, there were 45 mutation carriers, and 24 (53%) had atypical ATS phenotypes and 8 had none of them. They only showed abnormal U

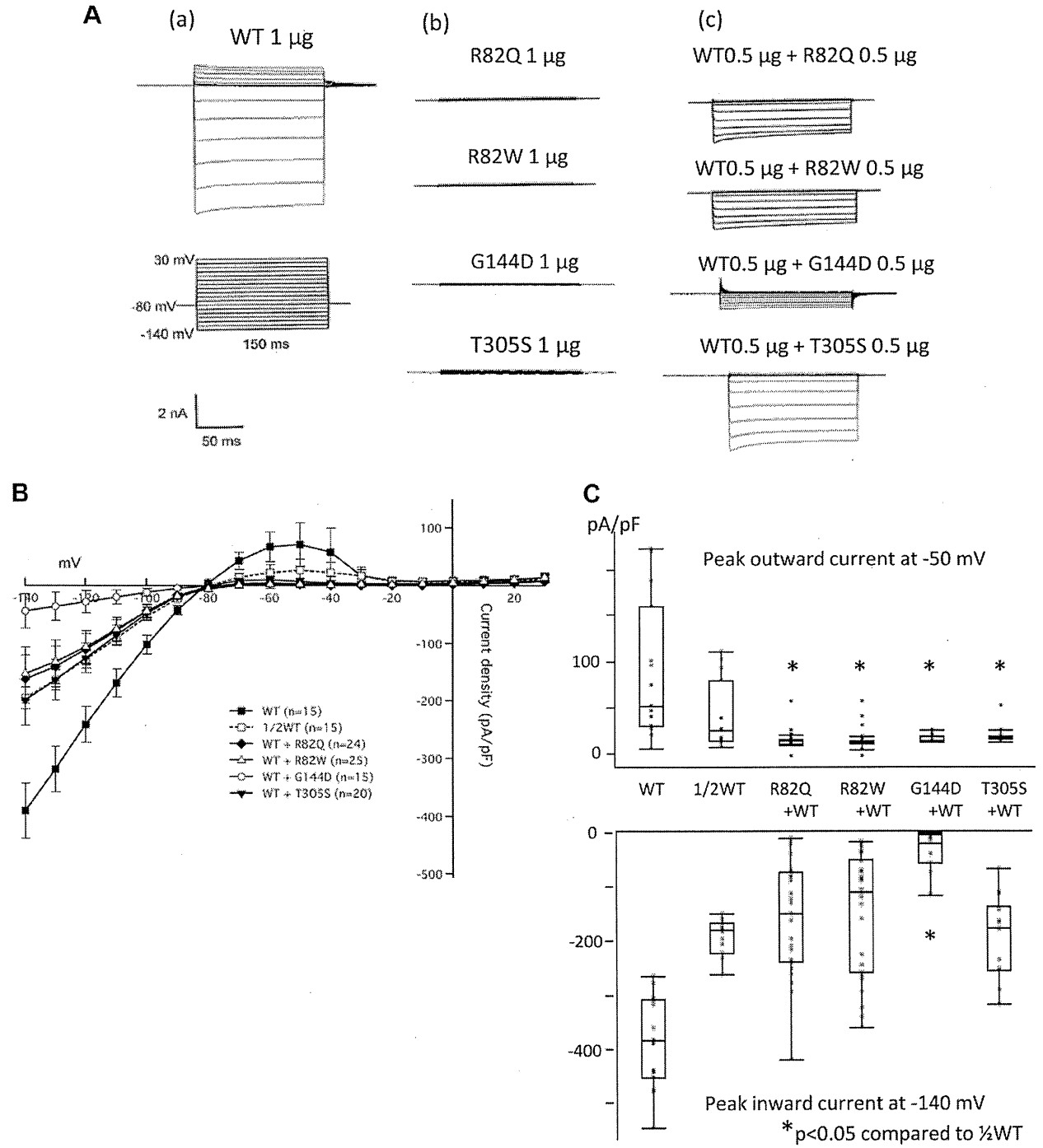

Figure 4. Functional analyses of mutated Kir2.1 channels found in group B. **A**, Representative Kir2.1 currents expressed in CHO cells: **a**, wild-type (WT) cDNA 1 μg; **b**, R82Q (1 μg), R82W (1 μg), G144D (1 μg), and T305S (1 μg). Cells were held at −80 mV. **c**, Cotransfection with WT (0.5 μg) and each mutant, R82Q (0.5 μg), R82W (0.5 μg), G144D (0.5 μg), and T305S (0.5 μg). Square pulses of 150-ms duration were applied to the potentials between −140 and +30 mV with 10-mV increments. Scale bars indicate 50 ms and 2 nA. **B**, Plots for current-voltage relationships obtained by multiple experiments of the same protocol as shown in **A**. Current densities were calculated by dividing with cell capacitance. **C**, Dot plots showing mean current densities in WT (1 μg, n=15), 1/2WT (0.5 μg, n=15), cotransfection with WT (0.5 μg) and R82Q (0.5 μg) (n=24), WT (0.5 μg) and R82W (0.5 μg) (n=25), WT (0.5 μg) and G144D (0.5 μg) (n=15), and WT (0.5 μg) and T305S (0.5 μg) (n=20). **Upper panel**, Those at −140 mV; **lower panel**, those at −50 mV.

waves. Accordingly, probands in this group received a genetic diagnosis at a significantly older age. Among the 3 features of ATS, dysmorphic features could be seen from the infant period; in contrast, ventricular arrhythmia appeared later, presumably because the I_{K1} current could be reduced in females by gonadal steroids.[29] The ATS-related phenotype was reported to be dependent on sex[30]—female subjects with *KCNJ2* R67W from a white family displayed ventricular

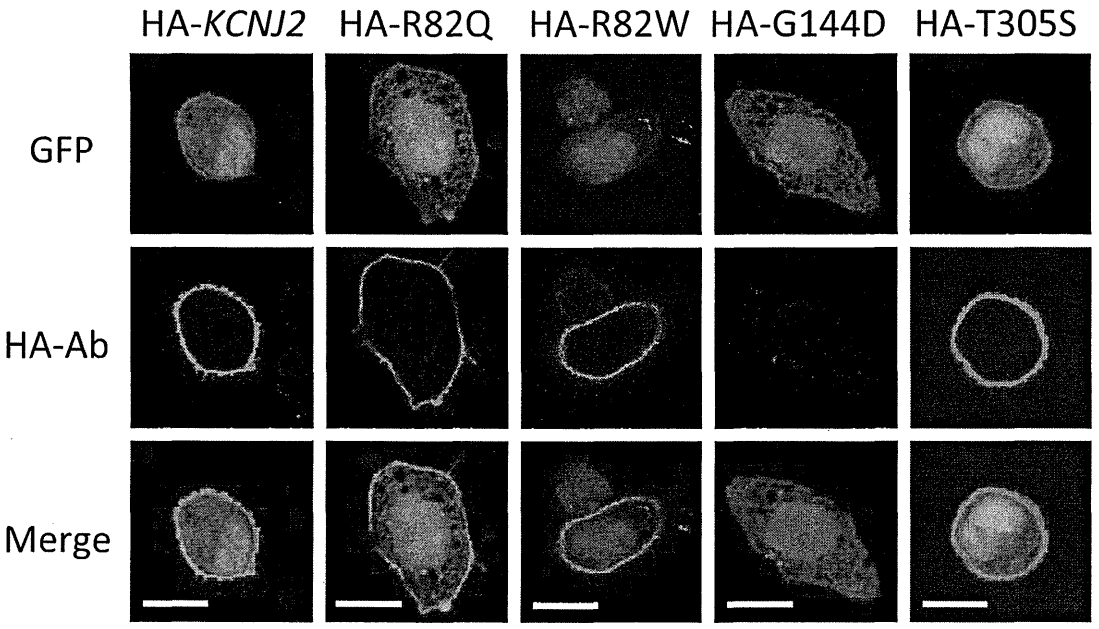

Figure 5. Cellular localization of wild-type (WT) and 4 mutant (R82Q, R82W, G144D, T305S) Kir2.1 channels. Hemagglutinin (HA)-*KCNJ2* indicates HA-tagged *KCNJ2* (positive control). **Upper panel** shows the green fluorescence of GFP; **middle panel**, red fluorescence of secondary anti-HA antibody; **lower panel**, merging of green and red fluorescences; **white bars** in the **merged panel** indicate 10 μm.

arrhythmias after the age of 10 years, and arrhythmias were reduced during pregnancy and after age 55 years, coinciding with menopause. In contrast, male mutation-positive subjects from the same family showed no ventricular arrhythmias but periodic paralysis. Interestingly, a case with R67W in our cohort was a male and complained of only periodic paralysis, supporting their conclusion, although there is a conflicting report by Donaldson et al.[26] They reported that the R67W mutation is capable of causing all phenotypes of ATS, and the pattern observed in the sex-specific kindred is not universal. It appears that other genetic or environmental factors contribute to a family's susceptibility to disease symptoms.

The topological location of *KCNJ2* mutations may influence the expression of ATS features. In the present study, C-terminal mutations were more frequent in the typical ATS group (Table 3). Zhang et al[14] also reported that dysmorphism and periodic paralysis were more frequently observed in C-terminal mutation carriers. The Kir 2.1 C-terminus relates to various types of loss of function in I_{K1} currents. Lopes et al[31] identified 12 basic residues in Kir2.1 that changed channel-PIP_2 interactions—10 of them were located in the C-terminus. The C-terminus also contains the endoplasmic reticulum (ER) export sequence, FCYENE, and the trafficking-related acidic cluster EEDDSE at positions 374 to 379 and 386 to 391, respectively.[32,33] More recently, we reported an S369X mutation located close to this ER export signal that impedes ER-Golgi transport.[7]

We tested the trafficking function of four mutations, and only G144D mutation showed a trafficking defect (Figure 5). Our results suggest that the phenotype expression variability of *KCNJ2* mutations may be influenced by the topological location of mutations; however, the other possibilities, for example, environmental factors, modifier genes, or SNPs,[34] remain unstudied.

Phenotypic Overlap Between CPVT and ATS

The prevalence of *KCNJ2* mutation carriers in the CPVT phenotype was lower than in the other phenotypes (Figure 1 and Table 1). Our 2 CPVT probands with *KCNJ2* mutation (G144D, T305S) had first syncope after the age of 30 years, and their ECGs showed bidirectional VT or PVCs at rest as well. In contrast, the age at first syncope of *RyR2*-related CPVT patients was reportedly younger age (mean age of 8 years),[10] and their syncope occurred mainly during exercise but not while resting. These findings, for example, late onset of symptoms and ventricular arrhythmia at rest, may be clues to distinguish between *KCNJ2*-related and *RyR2*- or *CASQ2*-related CPVT. Functional assays revealed that both G144D and T305S exerted dominant negative suppression effects on outward currents when coexpressed with WT Kir2.1 subunits. Apparently, therefore, baseline functional modulation by these mutations was not related to the phenotypic expression of ATS or CPVT.

Recently, a V227F mutation was identified in a patient with the typical CPVT phenotype but without dysmorphism or periodic paralysis.[35] A biophysical assay showed that heterozygous WT/V227F channels were identical to WT channels in function, but stimulation by cAMP-dependent protein kinase A (PKA) significantly downregulated the heterozygous mutant but not WT Kir2.1 currents. This particular type of loss-of-function may explain why the proband displayed the CPVT phenotype. More recently, Barajas-Martinez et al[36] demonstrated the characteristics of their patient with R260P mutation. She showed typical phenotypes of both ATS and CPVT. The β-blocker nadolol

was first used but ineffective. Her symptoms subsided after treatment with flecainide. She had dysmorphic features and bidirectional VT both at rest and during exercise testing. Functional analysis revealed that R260P mutation had strong dominant negative suppression effects, like that in our G144D case. Regarding our mutations, their modulation by PKA was not examined because they showed a significant loss-of-function at the baseline (Figure 4).

Phenotype and Channel Function

Although R82W, R82Q, G144D, and T305S were found in patients with an atypical phenotype of ATS (group B), these mutations showed dominant negative suppression effects on outward currents (Figure 4). Therefore, the results obtained for a heterologous expression system did not necessarily correlate with the clinical ATS severity. In this regard, Eckhardt et al[27] identified 4 *KCNJ2* mutations—R67Q, R82W, T75 mol/L, and T305A—in probands lacking the ATS triad and a family history of ATS. Surprisingly, we also identified R67W, R82W/Q, and T305S in group B. Therefore, residues of R67, R82, and T305 may be associated with atypical ATS phenotypes.

Study Limitations

Regarding CPVT probands, we screened 34 hot-spot exons of the *RyR2* gene. We could not exclude some variants in the remaining exons of *RyR2*. In conclusion, *KCNJ2* gene screening in patients with atypical ATS (only 1 of the ATS features or CPVT) phenotypes is of clinical importance, because 53% of mutation carriers were found to express atypical phenotypes, despite their severity of arrhythmia.

Acknowledgments

We are grateful to Dr Hitoshi Horigome, University of Tsukuba; Dr Norito Kokubun, Dokkyo Medical University; Dr Nobuyuki Murakoshi, University of Tsukuba; Dr Ichiro Niimura, Niimura Clinic; Dr Yuji Okuyama, Osaka University Graduate School of Medicine; Dr Takahiro Sato, Kanto Medical Center NTT East Corporation; Dr Yoshiaki Takahashi, Takahashi Pediatric and Cardiac Clinic; Dr Jun Yoshimoto, Shizuoka Children's Hospital; and Dr Masao Yoshinaga, National Hospital Organization Kagoshima Medical Center, for the contribution to this survey. We thank Arisa Ikeda for excellent technical assistance.

Sources of Funding

This work was supported by research grants from the Ministry of Education, Culture, Science, and Technology of Japan (to Dr Horie); National Natural Science Foundation of China (No. 30930105 to Dr Zhou and No 81170176 to Dr Zang); and health science research grants from the Ministry of Health, Labor, and Welfare of Japan for Clinical Research on Measures for Intractable Diseases (to Dr Horie).

Disclosures

None.

References

1. Andersen ED, Krasilnikoff PA, Overvad H. Intermittent muscular weakness, extrasystoles, and multiple developmental anomalies: a new syndrome? *Acta Paediatr Scand.* 1971;60:559–564.
2. Tawil R, Ptacek LJ, Pavlakis SG, DeVivo DC, Penn AS, Ozdemir C, et al. Andersen's syndrome: potassium-sensitive periodic paralysis, ventricular ectopy, and dysmorphic features. *Ann Neurol.* 1994;35:326–330.
3. Zaritsky JJ, Eckman DM, Wellman GC, Nelson MT, Schwarz TL. Targeted disruption of Kir2.1 and Kir2.2 genes reveals the essential role of the inwardly rectifying K(+) current in K(+)-mediated vasodilation. *Circ Res.* 2000;87:160–166.
4. Plaster NM, Tawil R, Tristani-Firouzi M, Canun S, Bendahhou S, Tsunoda A, et al. Mutations in Kir2.1 cause the developmental and episodic electrical phenotypes of Andersen's syndrome. *Cell.* 2001;105:511–519.
5. Ai T, Fujiwara Y, Tsuji K, Otani H, Nakano S, Kubo Y, et al. Novel *KCNJ2* mutation in familial periodic paralysis with ventricular dysrhythmia. *Circulation.* 2002;105:2592–2594.
6. Kobori A, Sarai N, Shimizu W, Nakamura Y, Murakami Y, Makiyama T, et al. Additional gene variants reduce effectiveness of beta-blockers in the LQT1 form of long QT syndrome. *J Cardiovasc Electrophysiol.* 2004;15:190–199.
7. Doi T, Makiyama T, Morimoto T, Haruna Y, Tsuji K, Ohno S, et al. A novel *KCNJ2* nonsense mutation, S369X, impedes trafficking and causes a limited form of Andersen-Tawil syndrome. *Circ Cardiovasc Genet.* 2011;4:253–260.
8. Haruna Y, Kobori A, Makiyama T, Yoshida H, Akao M, Doi T, et al. Genotype-phenotype correlations of *KCNJ2* mutations in Japanese patients with Andersen-Tawil syndrome. *Hum Mutat.* 2007;28:208.
9. Tester DJ, Arya P, Will M, Haglund CM, Farley AL, Makielski JC, et al. Genotypic heterogeneity and phenotypic mimicry among unrelated patients referred for catecholaminergic polymorphic ventricular tachycardia genetic testing. *Heart Rhythm.* 2006;3:800–805.
10. Priori SG, Napolitano C, Memmi M, Colombi B, Drago F, Gasparini M, et al. Clinical and molecular characterization of patients with catecholaminergic polymorphic ventricular tachycardia. *Circulation.* 2002;106:69–74.
11. McManis PG, Lambert EH, Daube JR. The exercise test in periodic paralysis. *Muscle Nerve.* 1986;9:704–710.
12. Tristani-Firouzi M, Jensen JL, Donaldson MR, Sansone V, Meola G, Hahn A, et al. Functional and clinical characterization of *KCNJ2* mutations associated with LQT7 (Andersen syndrome). *J Clin Invest.* 2002;110:381–388.
13. Bazett HC. An analysis of the time relations of electro-cardiograms. *Heart.* 1920;7:353–367.
14. Zhang L, Benson DW, Tristani-Firouzi M, Ptacek LJ, Tawil R, Schwartz PJ, et al. Electrocardiographic features in Andersen-Tawil syndrome patients with *KCNJ2* mutations: characteristic T-U-wave patterns predict the *KCNJ2* genotype. *Circulation.* 2005;111:2720–2726.
15. Yan GX, Antzelevitch C. Cellular basis for the normal T wave and the electrocardiographic manifestations of the long-QT syndrome. *Circulation.* 1998;98:1928–1936.
16. Keating M, Atkinson D, Dunn C, Timothy K, Vincent GM, Leppert M. Linkage of a cardiac arrhythmia, the long QT syndrome, and the Harvey Ras-1 gene. *Science.* 1991;252:704–706.
17. Lepeschkin E. The U wave of the electrocardiogram. *Mod Concepts Cardiovasc Dis.* 1969;38:39–45.
18. Jongbloed R, Marcelis C, Velter C, Doevendans P, Geraedts J, Smeets H. dHPLC analysis of potassium ion channel genes in congenital long QT syndrome. *Hum Mutat.* 2002;20:382–391.
19. George CH, Jundi H, Thomas NL, Fry DL, Lai FA. Ryanodine receptors and ventricular arrhythmias: emerging trends in mutations, mechanisms and therapies. *J Mol Cell Cardiol.* 2007;42:34–50.
20. Medeiros-Domingo A, Bhuiyan ZA, Tester DJ, Hofman N, Bikker H, van Tintelen JP, et al. The *RyR2*-encoded ryanodine receptor/calcium release channel in patients diagnosed previously with either catecholaminergic polymorphic ventricular tachycardia or genotype negative, exercise-induced long QT syndrome: a comprehensive open reading frame mutational analysis. *J Am Coll Cardiol.* 2009;54:2065–2074.
21. Itoh H, Shimizu W, Hayashi K, Yamagata K, Sakaguchi T, Ohno S, et al. Long QT syndrome with compound mutations is associated with a more severe phenotype: a Japanese multicenter study. *Heart Rhythm.* 2010;7:1411–1418.
22. Ohno S, Zankov DP, Yoshida H, Tsuji K, Makiyama T, Itoh H, et al. N- and C-terminal *KCNE1* mutations cause distinct phenotypes of long QT syndrome. *Heart Rhythm.* 2007;4:332–340.
23. Hosaka Y, Hanawa H, Washizuka T, Chinushi M, Yamashita F, Yoshida T, et al. Function, subcellular localization and assembly of a novel mutation of *KCNJ2* in Andersen's syndrome. *J Mol Cell Cardiol.* 2003;35:409–415.
24. Zankov DP, Yoshida H, Tsuji K, Toyoda F, Ding WG, Matsuura H, et al. Adrenergic regulation of the rapid component of delayed rectifier K+

current: implications for arrhythmogenesis in LQT2 patients. *Heart Rhythm*. 2009;6:1038–1046.
25. Yoshida H, Horie M, Otani H, Takano M, Tsuji K, Kubota T, et al. Characterization of a novel missense mutation in the pore of *HERG* in a patient with long QT syndrome. *J Cardiovasc Electrophysiol*. 1999;10: 1262–1270.
26. Donaldson MR, Jensen JL, Tristani-Firouzi M, Tawil R, Bendahhou S, Suarez WA, et al. PIP_2 binding residues of Kir2.1 are common targets of mutations causing Andersen syndrome. *Neurology*. 2003;60:1811–1816.
27. Eckhardt LL, Farley AL, Rodriguez E, Ruwaldt K, Hammill D, Tester DJ, et al. KCNJ2 mutations in arrhythmia patients referred for LQT testing: a mutation T305A with novel effect on rectification properties. *Heart Rhythm*. 2007;4:323–329.
28. Fodstad H, Swan H, Auberson M, Gautschi I, Loffing J, Schild L, et al. Loss-of-function mutations of the K(+) channel gene *KCNJ2* constitute a rare cause of long QT syndrome. *J Mol Cell Cardiol*. 2004;37:593–602.
29. Liu XK, Katchman A, Drici MD, Ebert SN, Ducic I, Morad M, et al. Gender difference in the cycle length-dependent QT and potassium currents in rabbits. *J Pharmacol Exp Ther*. 1998;285:672–679.
30. Andelfinger G, Tapper AR, Welch RC, Vanoye CG, George AL Jr, Benson DW. KCNJ2 mutation results in Andersen syndrome with sex-specific cardiac and skeletal muscle phenotypes. *Am J Hum Genet*. 2002;71:663–668.
31. Lopes CM, Zhang H, Rohacs T, Jin T, Yang J, Logothetis DE. Alterations in conserved Kir channel-PIP_2 interactions underlie channelopathies. *Neuron*. 2002;34:933–944.
32. Nehring RB, Wischmeyer E, Doring F, Veh RW, Sheng M, Karschin A. Neuronal inwardly rectifying K(+) channels differentially couple to PDZ proteins of the PSD-95/SAP90 family. *J Neurosci*. 2000;20:156–162.
33. Ma D, Zerangue N, Raab-Graham K, Fried SR, Jan YN, Jan LY. Diverse trafficking patterns due to multiple traffic motifs in g protein-activated inwardly rectifying potassium channels from brain and heart. *Neuron*. 2002;33:715–729.
34. Pfeufer A, Jalilzadeh S, Perz S, Mueller JC, Hinterseer M, Illig T, et al. Common variants in myocardial ion channel genes modify the qt interval in the general population: results from the KORA study. *Circ Res*. 2005;96:693–701.
35. Vega AL, Tester DJ, Ackerman MJ, Makielski JC. Protein kinase A-dependent biophysical phenotype for V227F-*KCNJ2* mutation in catecholaminergic polymorphic ventricular tachycardia. *Circ Arrhythm Electrophysiol*. 2009;2:540–547.
36. Barajas-Martinez H, Hu D, Ontiveros G, Caceres G, Desai M, Burashnikov E, et al. Biophysical and molecular characterization of a novel de novo *KCNJ2* mutation associated with Andersen-Tawil syndrome and catecholaminergic polymorphic ventricular tachycardia mimicry. *Circ Cardiovasc Genet*. 2011;4:51–57.

CLINICAL PERSPECTIVE

Mutations of *KCNJ2*, the gene encoding the human inward rectifier potassium channel Kir2.1, cause Andersen-Tawil syndrome (ATS), a disease exhibiting ventricular arrhythmia, periodic paralysis and dysmorphic features. However, some *KCNJ2* mutation carriers lack the ATS triad and sometimes share the phenotype of catecholaminergic polymorphic ventricular tachycardia (CPVT). We focused on the *KCNJ2* mutation carriers with "atypical ATS phenotype"—patients showing only 1 of ATS features and CPVT phenotype. We investigated the prevalence, clinical, and biophysical characteristics of "atypical ATS" phenotype in *KCNJ2* mutation carriers. *KCNJ2* screening were performed in 57 unrelated probands showing typical (≥2 ATS features) and atypical ATS. We identified 24 *KCNJ2* mutation carriers. Mutation-positive rates were 75% (15/20) in typical ATS, 71% (5/7) in ATS cardiac phenotype alone, 100% (2/2) in periodic paralysis alone, and 7% (2/28) in CPVT. Including 24 *KCNJ2* mutation-positive family members, we divided all carriers (n=45) into 2 groups: typical ATS (A) (n=21, 47%) and atypical phenotype (B) (n=24, 53%). Patients in (A) had a longer QUc interval and higher U-wave amplitude. C-terminal mutations were more frequent in (A). There were no significant differences in incidences of ventricular tachycardia. In patch-clamp analysis using heterologous expression system, the outward IK1 currents of 4 mutations found in (B) showed dominant negative suppression effect although their mild ATS phenotype. *KCNJ2* gene screening in atypical ATS phenotypes is of clinical importance, because more than half (53%) of mutation carriers express atypical phenotypes, despite their arrhythmia severity.

Circulation Journal
Official Journal of the Japanese Circulation Society
http://www.j-circ.or.jp

ORIGINAL ARTICLE
Arrhythmia/Electrophysiology

KCNE3 T4A as the Genetic Basis of Brugada-Pattern Electrocardiogram

Tadashi Nakajima, MD, PhD; Jie Wu, PhD; Yoshiaki Kaneko, MD, PhD; Takashi Ashihara, MD, PhD; Seiko Ohno, MD, PhD; Tadanobu Irie, MD; Wei-Guang Ding, MD, PhD; Hiroshi Matsuura, MD, PhD; Masahiko Kurabayashi, MD, PhD; Minoru Horie, MD, PhD

Background: Brugada syndrome (BrS) is genetically heterogeneous. In Japanese BrS patients, except for *SCN5A* and *KCNE5*, mutations in the responsible genes have not yet been identified, and therefore the genetic heterogeneity remains poorly elucidated.

Methods and Results: Forty consecutive patients with Brugada-pattern electrocardiogram (ECG) underwent comprehensive genetic analysis of BrS-causing genes including *SCN5A*, *SCN1B*, *SCN3B*, *CACNA1C*, *CACNB2*, *KCNE3* and *KCNE5*. Besides identifying 8 *SCN5A* mutations in the present cohort, a *KCNE3* T4A mutation was found in a 55-year-old male patient who had experienced several episodes of syncope. A head-up tilt test during passive tilt provoked both hypotension and bradycardia, followed by syncope. He was therefore diagnosed with neurally mediated syncope (NMS). To characterize the functional consequence of the mutant, electrophysiological experiments using whole-cell patch-clamp methods and computer simulations using human right ventricular wall model were carried out. It was found that KCNE3 T4A increased I_{to} recapitulated by heterologously coexpressing Kv4.3+KChIP2b+KCNE3-wild type or KCNE3-T4A in CHO cells.

Conclusions: A *KCNE3* T4A mutation was identified in a Japanese patient presenting Brugada-pattern ECG and NMS. Its functional consequence was the gain of function of I_{to}, which could underlie the pathogenesis of Brugada-pattern ECG. The data provide novel insights into the genetic basis of Japanese BrS. (*Circ J* 2012; **76:** 2763–2772)

Key Words: Brugada syndrome; I_{to}; *KCNE3*; Mutation; Neurally mediated syncope

Brugada syndrome (BrS) is a hereditable disorder characterized by ST-segment elevations in the right precordial electrocardiogram (ECG) leads, associated with a high incidence of syncope or sudden death due to ventricular tachyarrhythmias, which mostly affects men. BrS is genetically heterogeneous, and has been linked to mutations in genes that perturb cardiac ion currents (I_{Na}, I_{Ca}, $I_{K\text{-}ATP}$ and I_{to}) contributing to the early phase of action potential (AP).[1–12] Among the BrS-causing genes, mutations in *SCN5A* (encoding the pore-forming α-subunit of the cardiac voltage-gated sodium channel) have accounted for the major form of BrS in approximately 20% of cases, and other gene mutations for approximately 10%,[1–12] thus around 70% of BrS cases remain to be genetically elucidated.

The transient outward potassium current (I_{to}) in the heart functions mainly during the early phase of AP because it activates and inactivates rapidly on membrane depolarization. Predominant expression of I_{to} in ventricular epimyocardium compared to endomyocardium, especially in the right ventricle, contributes to the rapid repolarization and the initial plateau formation of the AP (AP notch).[13–15] Experimental studies suggested that the gain of function of I_{to} leads to augmentation of the AP notch in epimyocardium but not in endomyocardium, thus resulting in the enhancement of transmural voltage gradient during the ventricular repolarization, which is thought to be responsible for the ST-segment elevation in the right pre-

Received April 25, 2012; revised manuscript received July 26, 2012; accepted August 7, 2012; released online September 13, 2012 Time for primary review: 28 days

Department of Medicine and Biological Science, Gunma University Graduate School of Medicine, Maebashi (T.N., Y.K., T.I., M.K.); Department of Cardiovascular and Respiratory Medicine (J.W., T.A., S.O., M.H.), Department of Physiology (W.-G.D., H.M.), Shiga University of Medical Science, Otsu, Japan; and Department of Pharmacology, Medical School of Xi'an Jiaotong University, Xi'an, Shaanxi (J.W.), China

The first two authors contributed equally to this work (T.N., J.W.).

Mailing address: Minoru Horie, MD, PhD, Department of Cardiovascular and Respiratory Medicine, Shiga University of Medical Science, Seta Tsukinowa-cho, Otsu 520-2192, Japan. E-mail: horie@belle.shiga-med.ac.jp

ISSN-1346-9843 doi:10.1253/circj.CJ-12-0551

cordial ECG leads (Brugada-pattern ECG) in BrS.[14] Further augmentation of the AP notch in epimyocardium causes the loss of AP plateau phase (dome), which consequently leads to arrhythmogenesis in BrS defined as phase 2 reentry.[14] I_{to} in human ventricle is thought to be consist of α-subunit Kv4.3 (encoded by *KCND3*) and β-subunits including Kv channel interacting protein (KChIP), KCNE, diaminopeptidyl transferase-like protein (DPP) and Kvβ families.[16–24] Accordingly, mutations in the related genes that increase I_{to} may underlie the pathogenesis of BrS.

KCNE3, 1 member of the *KCNE* gene family (*KCNE1–5*), modulates the function of Kv4.3 as an inhibitory β-subunit.[19,20] Recently, Delpón et al identified a *KCNE3* R99H mutation in 1 BrS family.[6] Functional analysis using the heterologous expression system that recapitulates I_{to} by coexpression of Kv4.3 with KCNE3-wild type (WT)/R99H showed that KCNE3 R99H causes a gain of function of I_{to} by a dominant-positive effect, thus precipitating the development of BrS.[6] Moreover, mutations in Kv4.3 and *KCNE5*, which also functions as an inhibitory β-subunit of I_{to}, were identified in BrS patients.[9,10] Functional analysis of these mutations showed that they increase I_{to}.[9,10] Therefore, it was established that the gain of function of I_{to} by mutations in genes that encode I_{to} could be one of the causes of BrS.

We have previously reported the identification of 8 mutations in *SCN5A* among 30 consecutive Japanese patients with Brugada-pattern ECG.[25] Considering that the genetic heterogeneity of BrS is poorly elucidated in Japan,[10,26,27] we further conducted genetic screening of BrS-causing genes among the 30 consecutive patients and another 10 new patients with Brugada-pattern ECG, and identified a *KCNE3* T4A mutation in a patient presenting with neurally mediated syncope (NMS). In the present study, we describe the clinical phenotype of the *KCNE3* T4A carrier, and characterize the functional consequence of the I_{to} recapitulated by heterologously coexpressing Kv4.3+KChIP2b+KCNE3-T4A in CHO cells. Furthermore, we performed computer simulations based on the I_{to} obtained in electrophysiological recordings, and showed that KCNE3-T4A recapitulated the ECG phenotype.

Methods

Subjects

The present subjects were 40 consecutive patients (probands; 35 male, 47±16 years of age) with Brugada-pattern ECG who were referred to Gunma University Hospital between April 2002 and September 2010. All patients, except for patient 27, presented with coved-type ST-elevation in the right precordial ECG leads with or without provocation of Na channel blocker (pilsicainide: 1 mg/kg, or procainamide 5 mg/kg), although it is still under debate whether patients with drug-induced Brugada-pattern ECG have poor prognosis.[28,29] Echocardiography and conventional left catheterization, if performed, indicated no structural heart disease in all the patients. Thirty-two patients underwent electrophysiological assessment. Up to 3 extra stimuli (minimum coupling interval: 180 ms) were delivered from 2 ventricular sites (right ventricular apex and right ventricular outflow tract). A head-up tilt (HUT) test was performed using the same protocol as described previously.[30] Clinical features of the subjects are listed in **Table 1**.

Genetic Analysis

After obtaining appropriate approval from the institution review board and written informed consent from the patient, genomic DNA was extracted from peripheral blood lymphocytes using the standard protocol of the QIAamp DNA Blood Midi Kit (QIAGEN, Hilden, Germany). All coding exons of *SCN5A*, *SCN1B*, *KCNE3*, *SCN3B* and *KCNE5*, and their splice sites were amplified on polymerase chain reaction (PCR) using primers flanking the intronic sequences as reported previously.[1,5–7,25,31] The PCR products were purified and directly sequenced using an ABI PRISM 3130 Genetic Analyzer (Applied Biosystems, Foster City, CA, USA). Regarding patient 18, *CACNA1C* and *CACNB2* were also analyzed.[4] The mutation was analyzed twice on independent PCR amplification and sequencing. *KCNE3* T4A was not identified in 528 control alleles.

Heterologous Expression of hKv4.3 and β-Subunits in CHO Cells

Full-length cDNA fragment of WT KCNE3 in pCR3.1 vector was subcloned into pIRES-CD8 vector that is useful in cell selection. The KCNE3 mutant (T4A) was constructed using a Quick Change II XL site-directed mutagenesis kit according to the manufacturer's instructions (Stratagene, La Jolla, CA, USA) and subcloned to the same vector. The KCNE3 mutant was fully sequenced (ABI PRISM 3130 Genetic analyzer) to ensure fidelity. Full-length cDNA encoding the short isoform of human Kv4.3 (hKv4.3) subcloned into the pIRES-GFP (Clontech, Palo Alto, CA, USA) expression vector was kindly provided by Dr GF Tomaselli (Johns Hopkins University). Full-length cDNA encoding Kv channel-interacting protein 2b (KChIP2b) subcloned into the PCMV-IRS expression vector was a kind gift from Dr GN Tseng (Virginia Commonwealth University). Kv4.3 was transiently transfected into CHO cells together with KChIP2b and KCNE3-WT (or T4A) cDNA at equimolar ratio (Kv4.3, 1.0 μg; KChIP2b, 1.0 μg; KCNE3, 1.0 μg) using Lipofectamine (Invitrogen Life Technologies, Carlsbad, CA, USA) according to the manufacturer's instructions. In a subset of experiments, 0.5 μg KCNE3-WT and 0.5 μg KCNE3-T4A were co-transfected into cells with 1.0 μg Kv4.3 and 1.0 μg KChIP2b. The transfected cells were then cultured in Ham's F-12 medium (Nakalai Tesque, Kyoto, Japan) as described previously.[24]

Electrophysiologic Recording and Data Analysis

After 48 h of transfection, a coverslip with cells was transferred to a 0.5-ml bath chamber at 25°C on an inverted microscope stage and perfused at 1–2 ml/min with extracellular solution containing the following (in mmol/L): 140 NaCl, 5.4 KCl, 1.8 $CaCl_2$, 0.5 $MgCl_2$, 0.33 NaH_2PO_4, 5.5 glucose, and 5.0 HEPES; pH 7.4 with NaOH. Cells that emitted green fluorescence were chosen for patch-clamp experiments. If coexpressed with KCNE3 (or its mutant), the cells were incubated with polystyrene microbeads precoated with anti-CD8 antibody (Dynabeads M450, Dynal, Norway) for 15 min. In these cases, cells that emitted green fluorescence and had attached beads were chosen for electrophysiologic recording. Whole-cell membrane currents were recorded with an EPC-8 patch-clamp amplifier (HEKA, Lambrecht, Germany), and data were low-pass filtered at 1 kHz, acquired at 5 kHz through an LIH-1600 analog-to-digital converter (HEKA), and stored on hard disk using PulseFit software (HEKA). Patch pipettes had a resistance of 2.5–5.0 mol/LΩ when filled with the following pipette solution (in mmol/L): 70.0 potassium aspartate, 50.0 KCl, 10.0 KH_2PO_4, 1.0 $MgSO_4$, 3.0 Na_2-ATP (Sigma, Japan, Tokyo), 0.1 Li_2-GTP (Roche Diagnostics, Mannheim, Germany), 5.0 EGTA, and 5.0 HEPES (pH 7.2).

Whole cell currents were elicited in a series of depolarizing voltage steps from a holding potential of –80 mV. The time

Table 1. Clinical Features and Genetic Analysis in Brugada-Pattern ECG Patients

Patient no.	Sex	Age (years)	ECG	Symptom	FH	EPS	ICD	*SCN5A*	*SCN1B*	*SCN3B*	*KCNE3*	*KCNE5*
1	M	49	Coved (P)	Sy	No	VF	Yes	c.393–1 c>t**				
2	F	58	Coved	Asy	No	N/A	No	R1193Q				
3	M	36	Coved (P)	Asy	No	VF	No	A586T**				
4	M	29	Coved (P)	Sy	No	VF	Yes		L210P, S248R, R250T			
5	M	56	Coved	CPA	No	VF	Yes		L210P			
6	M	30	Coved	CPA	No	VF	Yes					
7	M	42	Coved (P)	Sy	No	No VF	Yes					
8	M	53	Coved (P)	CPA	No	No VF	Yes		R187H, L210P			
9	M	45	Coved	CPA	No	VF	Yes	P1090L	L210P, S248R, R250T			
10	M	47	Coved (P)	CPA	No	VF	Yes		L210P			
11	M	39	Coved (P)	Asy	No	NSVT	No		L210P			
12	M	32	Coved	Asy	Yes	N/A	Yes		L210P, S248R, R250T			
13	M	42	Coved (Pro)	Sy	No	VF	Yes	P1090L, R1232W				
14	M	59	Coved (P)	Asy	No	No VF	No	c.4437+5 g>a				
15	M	64	Coved	Asy	No	N/A	No		L210P*, S248R*, R250T*			
16	M	39	Coved (P)	Asy	No	NSVT	No					
17	M	61	Coved (P)	Asy	Yes	NSVT	No	R689H**				
18	M	55	Coved (P)	Sy	No	NSVT	No				T4A**	
19	M	37	Coved (P)	Sy	Yes	VF	Yes		L210P, S248R, R250T			
20	M	49	Coved (P)	Asy	No	No VF	No	H558R*, S1553R**				
21	F	38	Coved (P)	Asy	No	N/A	No					
22	M	64	Coved (P)	Asy	Yes	VF	Yes	H558R, R1193Q	L210P, S248R, R250T			
23	M	71	Coved (P)	CPA	No	No VF	Yes	P1090L	L210P*, S248R*, R250T*			
24	M	44	Coved (P)	Sy	Yes	VF	Yes	E1784K**				
25	M	56	Coved (P)	Sy	No	VF	Yes		L210P, S248R, R250T			
26	M	15	Coved	Sy	No	N/A	No		L210P*, S248R, R250T			
27	M	25	Saddle-back	Sy	Yes	No VF	Yes	V1951M**				
28	F	67	Coved (P)	Asy	No	N/A	No					
29	F	28	Coved	Asy	No	N/A	No	Q1706H**				
30	M	38	Coved	Sy	No	NSVT	No					
31	M	30	Coved (P)	Asy	No	No VF	No					
32	M	63	Coved (P)	Asy	No	NSVT	No		L210P, S248R, R250T			
33	M	43	Coved	Asy	No	VF	No					
34	M	57	Coved	Asy	No	No VF	No		L210P, S248R, R250T			
35	M	40	Coved (P)	Sy	No	VF	Yes		L210P, S248R, R250T			
36	M	66	Coved (P)	Sy	No	VF	Yes		L210P			
37	M	72	Coved (P)	Asy	No	VF	No		L210P, S248R, R250T			
38	M	33	Coved	Asy	No	NSVT	No					
39	M	77	Coved	Asy	No	VF	No		L210P, S248R, R250T			
40	F	15	Coved (P)	CPA	No	N/A	Yes	A735E**				

Mutations and non-synonymous variants are listed. *Homozygous; **mutations.
Asy, asymptomatic; CPA, cardiopulmonary arrest; ECG, electrocardiogram; EPS, up to 3 extrastimuli from right ventricular apex and right ventricular outflow tract; FH, family history of sudden death under age 45; N/A, not accessed; NSVT, non-sustained ventricular tachycardia; P, pilsicainide provocation; Pro, procainamide provocation; Sy, syncope; VF, ventricular fibrillation.

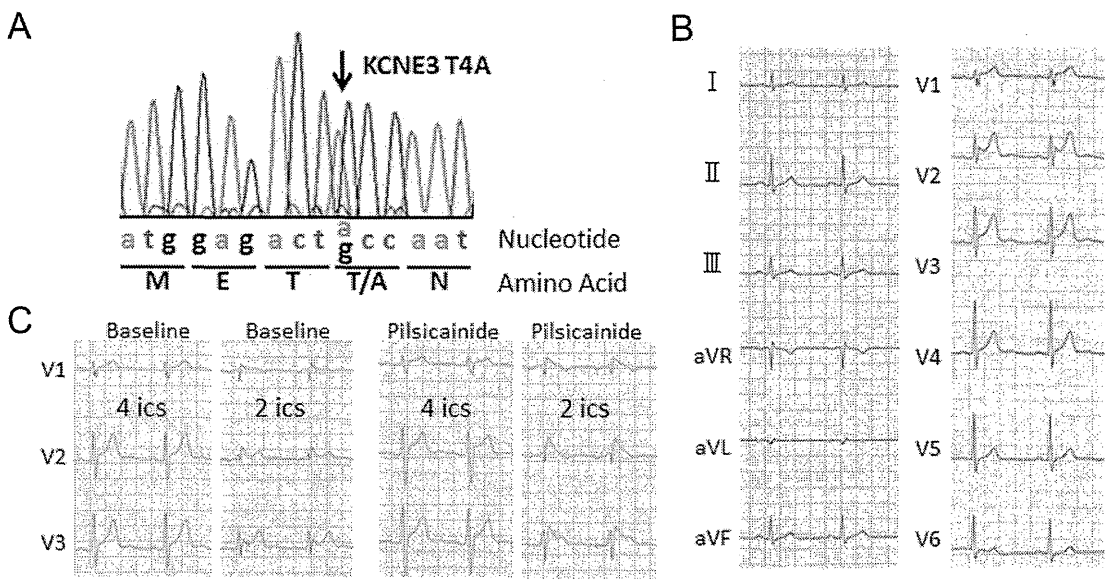

Figure 1. (A) Direct sequencing of the *KCNE3* gene in the index patient. Nucleotide and amino acid substitutions are indicated below. (B) Twelve-lead ECG recorded 2 months before admission. (C) V_{1-3} lead electrocardiogram before (baseline) and after pilsicainide provocation (Pilsicainide). ics, intercostal space.

interval between each voltage pulse was 10 s. The difference between the peak current amplitude and the current at the end of a test pulse was referred to as the transient outward current. To control for cell size variability, currents are expressed as densities (pA/pF) as described previously.[24] Steady-state activation curves were obtained by plotting the normalized conductance as a function of peak outward potentials. Steady-state inactivation curves were generated by a standard 2-pulse protocol with a conditioning pulse of 500 ms and obtained by plotting the normalized current as a function of the test potential. Steady-state inactivation/activation kinetics were fitted to the following Boltzmann equation:

$$Y(V)=1/(1+\exp[(V_{1/2}-V)/k]),$$

where Y = normalized conductance or current, $V_{1/2}$ = potential for half-maximum inactivation or activation, respectively, and k = slope factor.

Data relative to inactivation time constants, time to peak, and mean current levels were obtained using current data recorded at +50 mV. Recovery from inactivation was assessed using a standard paired-pulse protocol: a 1-s test pulse to +50 mV (P1) followed by a variable recovery interval at –80 mV and then a second test pulse to +50 mV (P2). Both the inactivation time constants and the time constant for recovery from inactivation were determined by fitting the data to a single exponential:

$$I(t)\ (\text{or } P2/P1)=A+B\exp(-t/\tau),$$

where I(t) = current amplitude at time t, A and B = constants, and τ = inactivation time constant or time constant for recovery from inactivation. For measurement of recovery from inactivation, the plot of P2/P1 instead of I(t) was used.

All data are given as mean±SEM. Statistical comparisons between 2 groups were analyzed using Student's unpaired t-test. Comparisons among multiple groups were analyzed using analysis of variance followed by Dunnett test. $P<0.05$ was considered significant.

Computer Simulation

To confirm the exact role of the *KCNE3* T4A mutation, we conducted simulations of paced propagation in a 0.5-cm 1-D bidomain myocardial model with transverse conductivity, mimicking transmural section of right ventricular wall. Membrane kinetics were represented by the Priebe-Beuckelmann human ventricular model,[32] of which original I_{to} was replaced by the I_{to} with KCNE3-WT or KCNE3-T4A mutation obtained in electrophysiologic recording.

To obtain the transmural gradient in the right ventricular wall, we defined endocardial and epicardial tissues as each of length 0.25 cm, and we set the conductances of the slowly activating component of the delayed rectifier potassium channel (I_{Ks}), the inward rectifier potassium channel (I_{K1}), and I_{to} in the endocardial layers to 46%, 82%, and 29%, respectively, of those in the epicardial layers. Pacing stimuli of 2 ms and strength twice-diastolic threshold were applied transmembranously to the endocardial end at a cycle length of 1,000 ms. The time and spatial discretization steps were 10 μs and 50 μm, respectively. Other model parameters and the numerical approach have been described elsewhere.[33]

Results

Genetic Analysis

We conducted comprehensive genetic analysis of BrS-causing genes including *SCN5A*, *SCN1B*, *KCNE3*, *SCN3B* and *KCNE5*, among 40 consecutive patients with Brugada-pattern ECG. Besides identifying 8 *SCN5A* mutations in the present cohort, we also found a T4A mutation in *KCNE3* in the patient 18 who had no mutations in the other genes (including *CACNA1C* and *CACNB2*) associated with BrS (**Figure 1A**; **Table 1**).

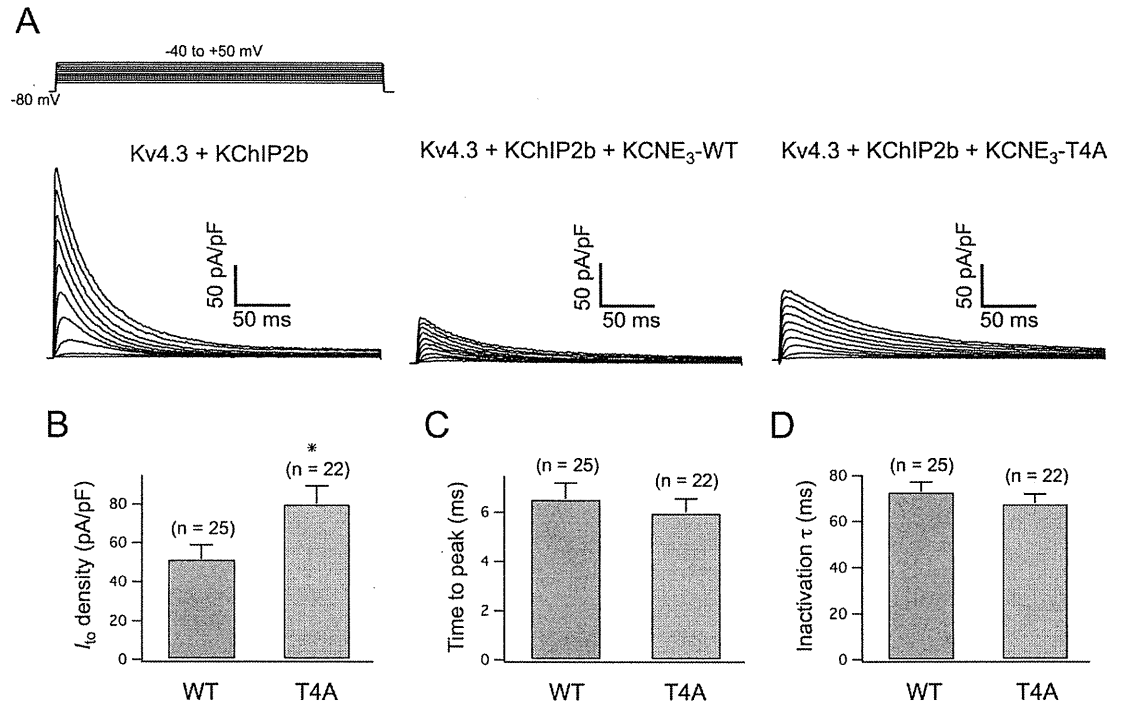

Figure 2. KCNE3-T4A increased I_{to} current reconstituted by coexpression of 1 μg Kv4.3 + 1 μg KChIP2b + 1 μg KCNE3 in CHO cells. (A) Representative current traces recorded from cells expressing (Left) Kv4.3 + KChIP2b, (Middle) Kv4.3 + KChIP2b + KCNE3-WT and (Right) Kv4.3 + KChIP2b + KCNE3-T4A. Inset, depolarizing test pulses introduced from −80 mV holding potential to potentials ranging from −40 to +50 mV, with 300-ms duration, in 10-mV increments. (B) Peak current density of I_{to}, (C) time to peak of activation course and (D) inactivation time constants recorded at +50 mV. (n), no. of experiments. *P<0.05 vs. WT.

Clinical Presentation

A 55-year-old man (patient 18) was referred to hospital to examine the cause of syncope. He had experienced several episodes of syncope under specific conditions, such as when sitting at a funeral, and standing up after drinking alcohol, since his 30 s. He had no previous history of illness except for syncopal episodes, and no family history of sudden cardiac death. A physical examination, chest X-ray, and blood test showed no remarkable abnormalities. His 12-lead ECG, recorded 2 months before admission, showed saddle-back-type ST-segment elevation in the right precordial ECG leads (**Figure 1B**). The QTc interval was 414 ms. A coved-type ST-segment elevation in the right precordial ECG leads at the second intercostal space appeared after provocation with pilsicainide (**Figure 1C**). Signal-averaged ECG showed no late potentials. Transthoracic echocardiography showed no apparent structural heart disease.

The patient underwent electrophysiological assessment. Up to 3 extrastimuli induced non-sustained polymorphic ventricular tachycardia, but not ventricular fibrillation. An HUT test was performed because syncopal episodes had occurred under specific conditions that could evoke NMS. The HUT test during passive tilt provoked both hypotension and bradycardia, followed by syncope. Therefore, the patient was diagnosed as having NMS. The patient was not prescribed medication or implanted with an implantable cardioverter defibrillator.

KCNE3-T4A Mutation Increased the Current Amplitude of the Kv4.3+KChIP2b+KCNE3 Channel

Because KCNE3 was shown to co-associate with Kv4.3 in the human heart, and I_{to} is thought to underlie the development of Brugada phenotype,[6,15] KCNE3-WT/T4A was coexpressed together with Kv4.3 and KChIP2b, which has been shown to serve as a principal β-subunit of I_{to}.[18,19,34,35] **Figure 2A** shows representative whole-cell current traces recorded from CHO cells expressing Kv4.3 + KChIP2b, Kv4.3 + KChIP2b + KCNE3-WT and Kv4.3 + KChIP2b + KCNE3-T4A.

Consistent with the previous literature, coexpression of KCNE3-WT dramatically reduced the current amplitude of the Kv4.3 + KChIP2b channel.[6,20,24] Further analysis of peak current showed that the current density of the coexpression with the KCNE3-T4A mutant was significantly larger than that for KCNE3-WT (Kv4.3 + KChIP2b + KCNE3-WT, 51.7±7.3 pA/pF, n=25 vs. Kv4.3 + KChIP2b + KCNE3-T4A, 80.2±9.1 pA/pF, n=22, P<0.05; **Figure 2A,B**). **Figure 2C** shows mean time interval from the onset of the pulse to maximum current (time to peak), and **Figure 2D** shows the time constants (τ) of inactivation obtained using a single exponential at +50 mV. These data indicate that KCNE3-T4A mutation increased the current amplitude of the Kv4.3 + KChIP2b + KCNE3 channel, but did not affect time to peak and the inactivation time course.

Effect of KCNE3-T4A on Activation/inactivation Kinetics of Kv4.3+KChIP2b+KCNE3 Channels

To further examine the effect of KCNE3-T4A on gating kinet-

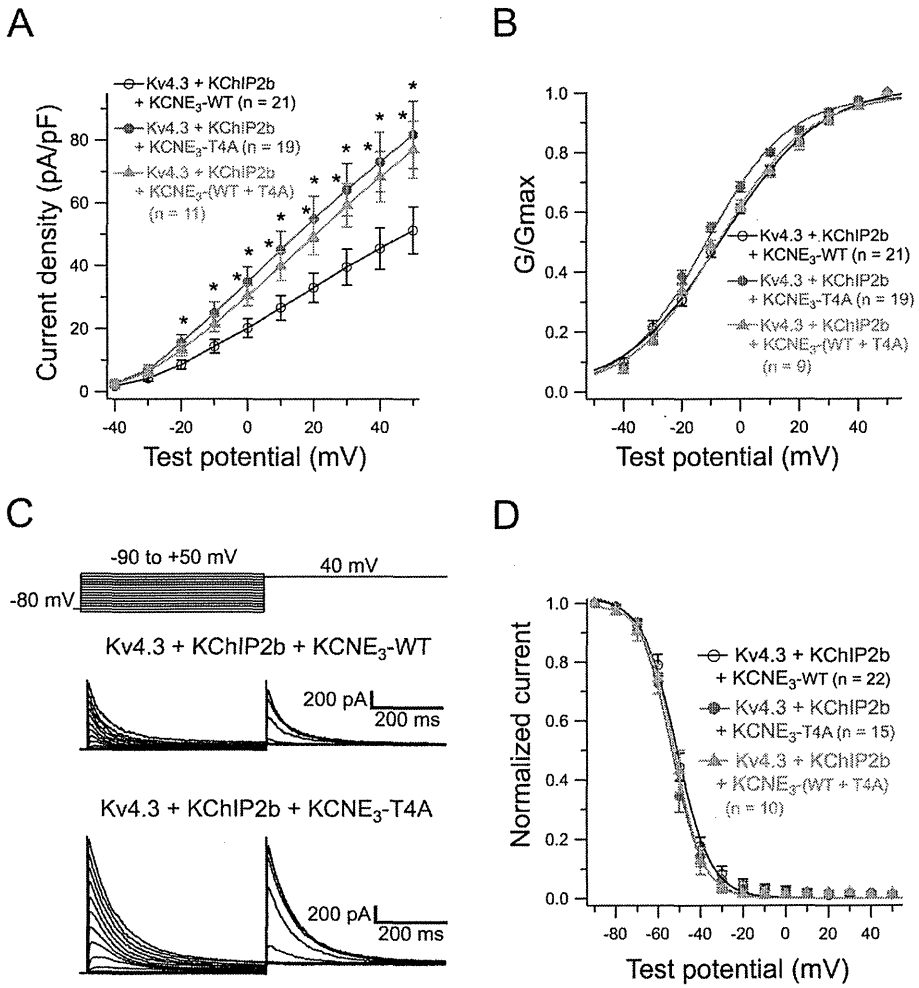

Figure 3. Effect of KCNE3-T4A on activation/inactivation kinetics of Kv4.3+KChIP2b+KCNE3 channels. (A) Current–voltage relationship curves showing peak current densities of the (open circles) Kv4.3+KChIP2b+KCNE3-WT, (closed circles) KCNE3-T4A and (filled triangles) KCNE3-(0.5 μg WT+0.5 μg T4A) channels. *P<0.05 vs. Kv4.3+KChIP2b+KCNE3-WT. (B) Normalized conductance-voltage relationships for peak currents in (A). (C) (Upper) Representative Kv4.3+KChIP2b+KCNE3-WT, (Lower) Kv4.3+KChIP2b+KCNE3-T4A current traces induced by 500-ms pre-pulses from –90 mV to +50 mV applied from the holding potential –80 mV in 10-mV steps followed by a second pulse to +40 mV (fixed) for assessing the inactivation process. (D) Steady-state inactivation curves for the (open circles) Kv4.3+KChIP2b+KCNE3-WT, (closed circles) KCNE3-T4A, and (filled triangles) KCNE3-(WT+T4A) channels. Peak currents thus measured were normalized by that obtained from the –90 mV pre-pulse and are plotted against the pre-pulse potentials. Smooth curves were drawn by fitting to the Boltzmann equation.

Table 2. Current Density and Biophysical Kinetics

	Current density	Activation	Steady-state activation		Steady-state inactivation		Inactivation	Recovery from inactivation
	At+50 mV (pA/pF)	Time to peak (ms)	$V_{1/2}$ (mV)	k (mV)	$V_{1/2}$ (mV)	k (mV)	τ (ms)	τ (ms)
Kv4.3+KChIP2b+KCNE3-WT	51.7±7.3 (n=25)	6.6±0.7 (n=25)	–6.5±2.0 (n=21)	17.2±1.1 (n=21)	–52.7±1.7 (n=22)	–9.9±1.7 (n=22)	73.0±4.2 (n=25)	65.7±10.2 (n=9)
Kv4.3+KChIP2b+KCNE3-T4A	80.2±9.1† (n=22)	6.0±0.6 (n=22)	–11.6±1.2† (n=19)	14.2±0.8 (n=19)	–54.7±1.6 (n=15)	–8.8±2.1 (n=15)	67.1±4.1 (n=22)	66.9±10.7 (n=9)
Kv4.3+KChIP2b+KCNE3-(WT+T4A)	77.7±8.6† (n=11)	6.7±0.8 (n=11)	–7.2±1.1 (n=10)	15.4±0.8 (n=10)	–52.2±2.0 (n=10)	–6.1±1.1 (n=10)	64.3±9.8 (n=11)	72.8±12.6 (n=6)

†P<0.05 vs. Kv4.3+KChIP2b+KCNE3-WT.

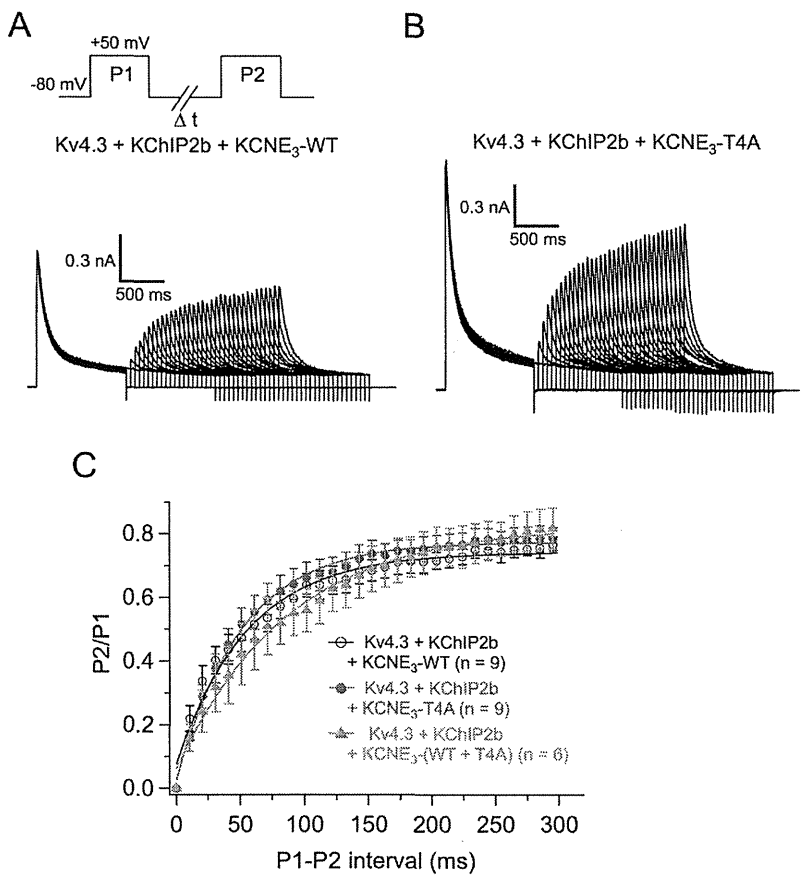

Figure 4. Effects of KCNE3-T4A on recovery from inactivation of the Kv4.3+KChIP2b+KCNE3 channel. A double step-pulse method was used to assess the recovery from inactivation. (A, inset) Protocol. A 1-s test pulse to +50 mV (P1) followed by a variable interval at –80 mV, then a second test pulse to +50 mV (P2). (A,B) Representative results from cells transfected with (A) Kv4.3+KChIP2b+KCNE3-WT and (B) Kv4.3+KChIP2b+KCNE3-T4A. (C) The time course of recovery of the (open circles) Kv4.3+KChIP2b+KCNE3-WT, (closed circles) KCNE3-T4A, and (filled triangles) KCNE3-(WT+T4A) channels. The ratio to peak current amplitude (P2/P1) is plotted as a function of the inter-pulse (P1–P2) interval.

ics of Kv4.3+KChIP2b+KCNE3 channel, we assessed the current-voltage (I–V) relationship of the Kv4.3+KChIP2b+KCNE3-T4A and Kv4.3+KChIP2b+KCNE3-WT+KCNE3-T4A channels. Coexpression of KCNE3-T4A (at –20 to +50 mV) or KCNE3-WT+KCNE3-T4A (at 0 to +50 mV) significantly increased peak current densities (**Figure 3A**; **Table 2**). Meanwhile, coexpression of KCNE3-T4A, but not KCNE3-(T4A+WT), also caused a negative shift (approximately –5 mV) of voltage dependence of steady-state activation as assessed by plotting the normalized conductance as a function of test potentials (**Figure 3B**; **Table 2**).

Figure 3C shows the representative current traces elicited by a double-step pulse method (inset) used to evaluate steady-state inactivation. Peak currents recorded at various levels of pre-pulse (**Figure 3C**) were normalized by that measured after a 500-ms pre-pulse at –90 mV and plotted as a function of pre-pulse test potentials (**Figure 3D**). Coexpression of KCNE3-T4A or KCNE3-(WT+T4A) with Kv4.3+KChIP2b did not significantly modify the steady-state inactivation of Kv4.3+KChIP2b+KCNE3 channels (**Figure 3D**; **Table 2**).

Because the changes in the time course of reactivation can also affect I_{to} current, a double-pulse protocol (**Figure 4A**) was used to test the effect of KCNE3-T4A or KCNE3-(WT+T4A) coexpression on the time course for recovery from inactivation. **Figures 4A,B** shows the representative current traces for coexpression of KCNE3-WT and KCNE3-T4A. **Figure 4C** shows the time courses of recovery of KCNE3-WT, KCNE3-T4A and KCNE3-(WT+T4A) coexpression together with Kv4.3+KChIP2b. Time constants (τ) of recovery from inactivation are listed in **Table 2**. Coexpression of KCNE3-T4A or KCNE3-(WT+T4A) did not affect the time course of recovery from inactivation.

Phenotype of KCNE3-T4A Mutation in a Simulated Human Right Ventricular Wall Model

To clarify whether the gain of function of I_{to} resulting from KCNE3-T4A mutation is indeed responsible for the Brugada-pattern ECG, we performed computer simulations using the 1-D myocardial model of human right ventricular wall. Based on the I_{to} obtained in electrophysiologic recording (**Figures 3A,B,D**), we numerically reproduced the current-voltage relationship curves (**Figure 5A**), the normalized conductance-voltage relationship curves (**Figure 5B**), and the steady-state inactivation curves (**Figure 5C**) of the KCNE3-WT and KCNE3-T4A channels. The numerically reproduced I_{to} was incorporated into the 1-D right ventricular wall model, consisting of endocardial and epicardial layers (**Figure 5D**). We found that the difference in the phase 2 AP between endocardial and epicardial layers in the KCNE3-T4A model was larger than that in the KCNE3-WT model, and therefore the simulated right precordial ECG showed ST-segment elevation in the case of KCNE3-T4A (**Figure 5E**).

To examine the adequacy of the KCNE3-T4A model, we additionally conducted simulations with sodium channel blockade. In the case of KCNE3-WT (**Figure 5F**), because sodium channel block (I_{Na} 50%) did not increase the difference in phase

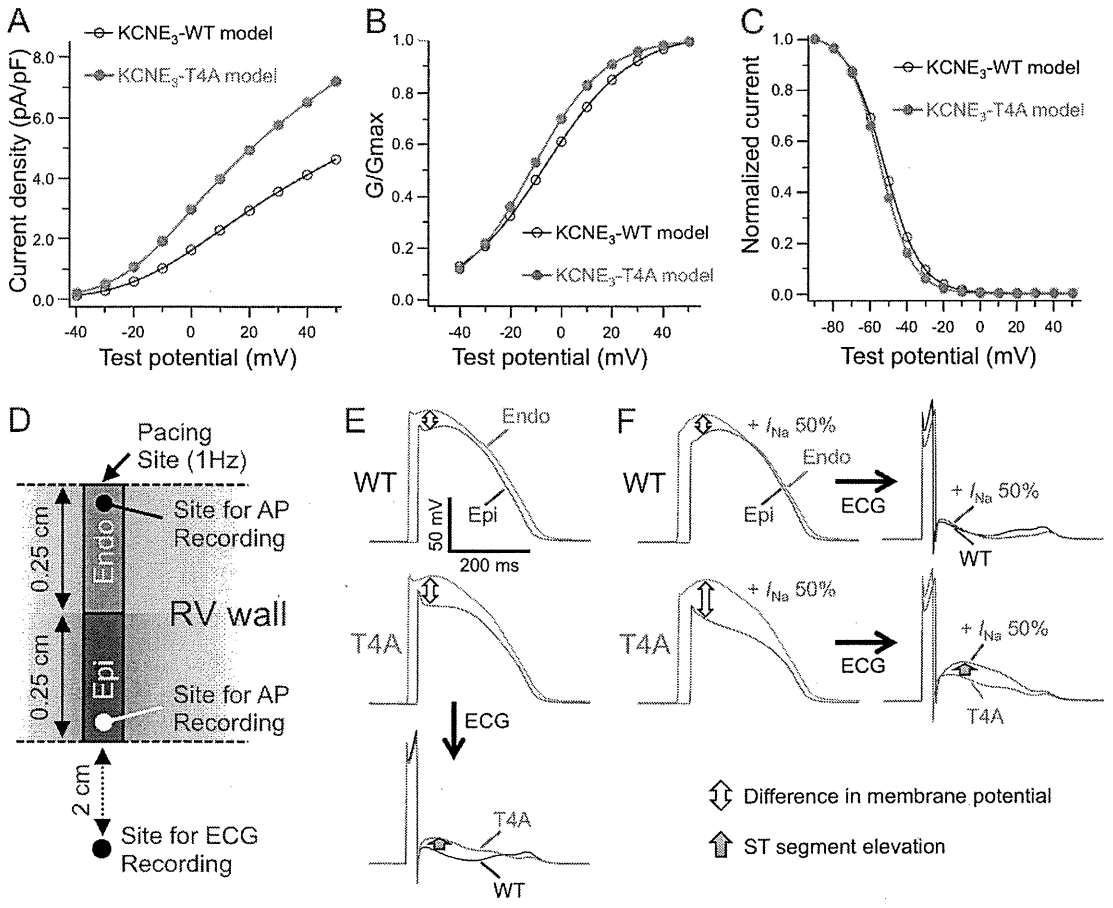

Figure 5. (A–C) Numerically reproduced (A) current-voltage relationship curves, (B) normalized conductance-voltage relationship curves, and (C) steady-state inactivation curves of KCNE3-WT and KCNE3-T4A models. (D) One-dimensional bidomain myocardial computer model, representing the electrical behaviors of the right ventricular wall. The sites for pacing and recording action potential (AP) and electrocardiogram (ECG) are shown. (E) Influence of KCNE3-T4A mutation on both AP and ECG. Endo, endocardial layer; Epi, epicardial layer. (F) Effect of sodium channel blockade (I_{Na} 50%) on both AP and ECG in KCNE3-WT and KCNE3-T4A cases.

1 AP between endocardial and epicardial layers, no ST-segment elevation was observed in the simulated ECG. In contrast, in the case of KCNE3-T4A (**Figure 5F**), the same sodium channel block caused the loss of dome of AP in the epicardial layer rather than the endocardial layer, and therefore the simulated ECG showed marked ST-segment elevation, consistent with clinical observation (**Figure 1C**).

Discussion

We identified a *KCNE3* T4A mutation among 40 consecutive patients with Brugada-pattern ECG. The index patient had experienced several episodes of syncope, possibly due to NMS rather than BrS-related ventricular tachyarrhythmias.

The gain of function of I_{to} by mutations in genes that encode I_{to} had been thought to cause BrS.[14,15] Indeed, an R99H mutation in *KCNE3* was recently identified in 1 BrS family.[6] Functional analysis of I_{to} reconstituted by Kv4.3/KCNE3-R99H showed a gain of function of the channel with a dominant-positive effect. Moreover, the mutation was co-segregated with ECG phenotype.[6] Therefore, the mutation underlies the development of BrS. *KCNE3* T4A, the variant identified in the present cohort, could be a candidate for another *KCNE3* mutation that is associated with BrS.

We reconstituted I_{to} by coexpressing Kv4.3 with KCNE3+KChIP2b in CHO cells, and examined the functional consequence of KCNE3-T4A, because KChIP2 associates with Kv4 and increases Kv4 current with the increase of surface expression of Kv4, by facilitating the trafficking of the channel and the kinetic changes that more resemble native I_{to}.[35] KCNE3-T4A also increased I_{to} with a dominant-positive effect. Moreover, computer simulations based on the I_{to} obtained in electrophysiological recordings demonstrated that KCNE3-T4A recapitulated the ECG phenotype in the present case. These results indicate that *KCNE3* T4A could underlie the pathogenesis of Brugada-pattern ECG. Although it may be required to demonstrate a co-segregation of *KCNE3* T4A with ECG phenotype to validate that the *KCNE3* T4A is associated with Brugada-pattern ECG, we unfortunately could not investigate the patient's family members because of lack of consent.

The precise molecular mechanisms of the reverse of KCNE3-induced suppression of Kv4.3 by KCNE3-T4A remain to be elucidated. Delpón et al demonstrated, using coimmunoprecipitation techniques, that KCNE3 coassociates with Kv4.3 in human atrial myocardium and rat ventricular myocardium.[6] In addition, Lundby and Olesen reported that KCNE3 has an inhibitory effect on Kv4.3 independent of the presence of KChIP2 in a heterologous expression system.[20] Therefore, although we recapitulated I_{to} in the presence of KChIP2b, KCNE3-T4A might reverse the KCNE3-induced suppression of Kv4.3 in the absence of KChIP2b, as is the case with KCNE3-R99H reported by Delpón et al.[6] Interestingly, Lundby and Olesen also reported that delayed injection of KCNE3 into *Xenopus* oocytes can almost completely inhibit Kv4.3 current, suggesting that KCNE3 transcription can act as a regulatory mechanism of the Kv4.3 current density.[20] Further studies of the transcription, trafficking and turnover rate of K4.3 channel and channel complexes in the presence or absence of KChIP2b and KCNE3-WT/T4A, would be required to elucidate the mechanisms of the reverse of KCNE3-induced suppression of I_{to} by KCNE3-T4A.

Yokokawa et al reported that 35% of patients with Brugada-pattern ECG had positive responses during the HUT test,[30] demonstrating a high prevalence of NMS among individuals with Brugada-pattern ECG. Although the autonomic nervous system may play an important role in the development of both BrS and NMS, the precise pathophysiological link between BrS and NMS remains to be elucidated. The identification of a novel *SCN5A* Q55X mutation in a patient with Brugada-pattern ECG presenting as NMS and the expression of *SCN5A* in both myocardial cells and intracardiac ganglia raise the possibility of a genetic association between BrS and NMS.[36,37] *KCNE3* (MiRP2) is also expressed in not only the heart but also the central nervous system, and it modulates delayed rectifier currents in mammalian neurons by forming native channel complexes with Kv2.1 and Kv3.1b.[38] Taken together, *KCNE3* T4A may be associated with both phenotypes of BrS and NMS.

In contrast, we have previously reported that *KCNE3* mutations (R99H and T4A) are associated with long QT syndrome (LQTS).[39] A functional analysis of KCNQ1+KCNE3-R99H coexpression demonstrated a reduction of the repolarizing potassium current, thus supporting the proposition that *KCNE3* R99H could be a cause of LQTS. A functional analysis of KCNQ1+KCNE3-T4A, however, could not demonstrate significant functional abnormalities. Regarding the present case, the QTc interval was not prolonged. Therefore, further studies would be necessary to establish the association between *KCNE3* T4A and LQTS. Along with this line, 2 *KCNE3* T4A carriers we previously reported had no apparent spontaneous ST-segment elevation in the right precordial ECG leads.[39] One carrier was a 16-year-old boy, much younger than most affected patients, and another was an old woman. Pharmacological provocation tests were not performed to study whether they had Brugada-pattern ECG.

Conclusions

We identified a *KCNE3* T4A mutation in a Japanese patient with Brugada-pattern ECG presenting as NMS. Its functional consequence was the gain of function of I_{to}, which could underlie the pathogenesis of Brugada-pattern ECG. The data provide novel insight into the genetic basis of Japanese BrS. Further studies are required to clarify whether the *KCNE3* T4A mutation is also associated with NMS and/or LQTS.

Acknowledgments

We thank the patients for their participation in this study. We thank Takako Kobayashi and Yukiyo Tosaka for helping with the genetic analysis. This work was supported, in part, by a Grant-in-Aid for Scientific Research from the Ministry of Education, Culture, Sports, Science and Technology (to T.N. and M.H.). This work was also supported by grants from the Uehara Memorial Foundation and the Ministry of Health, Labor and Welfare of Japan for Clinical Research on Measures for Intractable Diseases (to M.H.), and the National Natural Science Foundation of China (#81273501 to J.W. and W.G.D.).

Disclosures

Conflict of interest to declare: None.

References

1. Chen Q, Kirsch GE, Zhang D, Brugada R, Brugada J, Brugada P, et al. Genetic basis and molecular mechanism for idiopathic ventricular fibrillation. *Nature* 1998; **392:** 293–296.
2. London B, Michalec M, Mehdi H, Zhu X, Kerchner L, Sanyal S, et al. Mutation in glycerol-3-phosphate dehydrogenase 1 like gene (GPD1-L) decreases cardiac Na+ current and causes inherited arrhythmias. *Circulation* 2007; **116:** 2260–2268.
3. Van Norstrand DW, Valdivia CR, Tester DJ, Ueda K, London B, Makielski JC, et al. Molecular and functional characterization of novel glycerol-3-phosphate dehydrogenase 1 like gene (GPD1-L) mutations in sudden infant death syndrome. *Circulation* 2007; **116:** 2253–2259.
4. Antzelevitch C, Pollevick GD, Cordeiro JM, Casis O, Sanguinetti MC, Aizawa Y, et al. Loss-of-function mutations in the cardiac calcium channel underlie a new clinical entity characterized by ST-segment elevation, short QT intervals, and sudden cardiac death. *Circulation* 2007; **115:** 442–449.
5. Watanabe H, Koopmann TT, Le Scouarnec S, Yang T, Ingram CR, Schott JJ, et al. Sodium channel beta1 subunit mutations associated with Brugada syndrome and cardiac conduction disease in humans. *J Clin Invest* 2008; **118:** 2260–2268.
6. Delpón E, Cordeiro JM, Núñez L, Thomsen PE, Guerchicoff A, Pollevick GD, et al. Functional effects of KCNE3 mutation and its role in the development of Brugada syndrome. *Circ Arrhythm Electrophysiol* 2008; **1:** 209–218.
7. Hu D, Barajas-Martinez H, Burashnikov E, Springer M, Wu Y, Varro A, et al. A mutation in the beta 3 subunit of the cardiac sodium channel associated with Brugada ECG phenotype. *Circ Cardiovasc Genet* 2009; **2:** 270–278.
8. Kattygnarath D, Maugenre S, Neyroud N, Balse E, Ichai C, Denjoy I, et al. MOG1: A new susceptibility gene for Brugada syndrome. *Circ Cardiovasc Genet* 2011; **4:** 261–268.
9. Giudicessi JR, Ye D, Tester DJ, Crotti L, Mugione A, Nesterenko VV, et al. Transient outward current (I(to)) gain-of-function mutations in the KCND3-encoded Kv4.3 potassium channel and Brugada syndrome. *Heart Rhythm* 2011; **8:** 1024–1032.
10. Ohno S, Zankov DP, Ding WG, Itoh H, Makiyama T, Doi T, et al. KCNE5 (KCNE1L) variants are novel modulators of Brugada syndrome and idiopathic ventricular fibrillation. *Circ Arrhythm Electrophysiol* 2011; **4:** 352–361.
11. Barajas-Martinez H, Hu D, Ferrer T, Onetti CG, Wu Y, Burashnikov E, et al. Molecular genetic and functional association of Brugada and early repolarization syndromes with S422L missense mutation in KCNJ8. *Heart Rhythm* 2012; **9:** 548–555.
12. Antzelevitch C. Genetic, molecular and cellular mechanisms underlying the J wave syndromes. *Circ J* 2012; **76:** 1054–1065.
13. Nabauer M, Beuckelmann DJ, Uberfuhr P, Steinbeck G. Regional differences in current density and rate-dependent properties of the transient outward current in subepicardial and subendocardial myocytes of human left ventricle. *Circulation* 1996; **93:** 168–177.
14. Yan GX, Antzelevitch C. Cellular basis for the Brugada syndrome and other mechanisms of arrhythmogenesis associated with ST-segment elevation. *Circulation* 1999; **100:** 1660–1666.
15. Antzelevitch C. Brugada syndrome. *Pacing Clin Electrophysiol* 2006; **29:** 1130–1159.
16. Dixon JE, Shi W, Wang HS, McDonald C, Yu H, Wymore RS, et al. Role of the Kv4.3 K+ channel in ventricular muscle: A molecular correlate for the transient outward current. *Circ Res* 1996; **79:** 659–668.
17. Kuo HC, Cheng CF, Clark RB, Lin JJ, Lin JL, Hoshijima M, et al. A defect in the Kv channel-interacting protein 2 (KChIP2) gene leads to a complete loss of I(to) and confers susceptibility to ventricular tachycardia. *Cell* 2001; **107:** 801–813.

18. Decher N, Uyguner O, Scherer CR, Karaman B, Yuksel-Apak M, Busch AE, et al. hKChIP2 is a functional modifier of hKv4.3 potassium channels: Cloning and expression of a short hKChIP2 splice variant. *Cardiovasc Res* 2001; **52:** 255–264.
19. Radicke S, Cotella D, Graf EM, Banse U, Jost N, Varro A, et al. Functional modulation of the transient outward current Ito by KCNE beta-subunits and regional distribution in human non-failing and failing hearts. *Cardiovasc Res* 2006; **71:** 695–703.
20. Lundby A, Olesen SP. KCNE3 is an inhibitory subunit of the Kv4.3 potassium channel. *Biochem Biophys Res Commun* 2006; **346:** 958–967.
21. Radicke S, Cotella D, Graf EM, Ravens U, Wettwer E. Expression and function of dipeptidyl-aminopeptidase-like protein 6 as a putative beta-subunit of human cardiac transient outward current encoded by Kv4.3. *J Physiol* 2005; **565:** 751–756.
22. Aimond F, Kwak SP, Rhodes KJ, Nerbonne JM. Accessory Kvbeta1 subunits differentially modulate the functional expression of voltage-gated K+ channels in mouse ventricular myocytes. *Circ Res* 2005; **96:** 451–458.
23. Niwa N, Nerbonne JM. Molecular determinants of cardiac transient outward potassium current (I(to)) expression and regulation. *J Mol Cell Cardiol* 2010; **48:** 12–25.
24. Wu J, Shimizu W, Ding WG, Ohno S, Toyoda F, Itoh H, et al. KCNE2 modulation of Kv4.3 current and its potential role in fatal rhythm disorders. *Heart Rhythm* 2010; **7:** 199–205.
25. Nakajima T, Kaneko Y, Saito A, Irie T, Tange S, Iso T, et al. Identification of six novel SCN5A mutations in Japanese patients with Brugada syndrome. *Int Heart J* 2011; **52:** 27–31.
26. Ogawa R, Kishi R, Takagi A, Sakaue I, Takahashi H, Matsumoto N, et al. A novel microsatellite polymorphism of sodium channel beta1-subunit gene (SCN1B) may underlie abnormal cardiac excitation manifested by coved-type ST-elevation compatible with Brugada syndrome in Japanese. *Int J Clin Pharmacol Ther* 2010; **48:** 109–119.
27. Makiyama T, Akao M, Haruna Y, Tsuji K, Doi T, Ohno S, et al. Mutation analysis of the glycerol-3 phosphate dehydrogenase-1 like (GPD1L) gene in Japanese patients with Brugada syndrome. *Circ J* 2008; **72:** 1705–1706.
28. Shimizu A. Is this a philosophic issue? Do patients with drug-induced Brugada type ECG have poor prognosis? (Pro) *Circ J* 2010; **74:** 2455–2463.
29. Nishizaki M, Sakurada H, Yamawake N, Ueda-Tatsumoto A, Hiraoka M. Low risk for arrhythmic events in asymptomatic patients with drug-induced type 1 ECG. Do patients with drug-induced Brugada type ECG have poor prognosis? (Con) *Circ J* 2010; **74:** 2464–2473.
30. Yokokawa M, Okamura H, Noda T, Satomi K, Suyama K, Kurita T, et al. Neurally mediated syncope as a cause of syncope in patients with Brugada electrocardiogram. *J Cardiovasc Electrophysiol* 2010; **21:** 186–192.
31. Nakajima T, Kaneko Y, Irie T, Takahashi R, Kato T, Iijima T, et al. Compound and digenic heterozygosity in desmosome genes as a cause of arrhythmogenic right ventricular cardiomyopathy in Japanese patients. *Circ J* 2012; **76:** 737–743.
32. Priebe L, Beuckelmann DJ. Simulation study of cellular electric properties in heart failure. *Circ Res* 1998; **82:** 1206–1223.
33. Tsuji-Wakisaka K, Akao M, Ishii TM, Ashihara T, Makiyama T, Ohno S, et al. Identification and functional characterization of KCNQ1 mutations around the exon 7-intron 7 junction affecting the splicing process. *Biochim Biophys Acta* 2011; **1812:** 1452–1459.
34. Wang S, Bondarenko VE, Qu Y, Morales MJ, Rasmusson RL, Strauss HC. Activation properties of Kv4.3 channels: Time, voltage and [K+]o dependence. *J Physiol* 2004; **557:** 705–717.
35. An WF, Bowlby MR, Betty M, Cao J, Ling HP, Mendoza G, et al. Modulation of A-type potassium channels by a family of calcium sensors. *Nature* 2000; **403:** 553–556.
36. Makita N, Sumitomo N, Watanabe I, Tsutsui H. Novel SCN5A mutation (Q55X) associated with age-dependent expression of Brugada syndrome presenting as neurally mediated syncope. *Heart Rhythm* 2007; **4:** 516–519.
37. Scornik FS, Desai M, Brugada R, Guerchicoff A, Pollevick GD, Antzelevitch C, et al. Functional expression of "cardiac-type" Nav1.5 sodium channel in canine intracardiac ganglia. *Heart Rhythm* 2006; **3:** 842–850.
38. McCrossan ZA, Lewis A, Panaghie G, Jordan PN, Christini DJ, Lerner DJ, et al. MinK-related peptide 2 modulates Kv2.1 and Kv3.1 potassium channels in mammalian brain. *J Neurosci* 2003; **23:** 8077–8091.
39. Ohno S, Toyoda F, Zankov DP, Yoshida H, Makiyama T, Tsuji K, et al. Novel KCNE3 mutation reduces repolarizing potassium current and associated with long QT syndrome. *Hum Mutat* 2009; **30:** 557–563.

Circulation Journal
Official Journal of the Japanese Circulation Society
http://www.j-circ.or.jp

ORIGINAL ARTICLE
Arrhythmia/Electrophysiology

Prognostic Implications of Progressive Cardiac Conduction Disease

Tamiro Kawaguchi, MD; Hideki Hayashi, MD, PhD; Akashi Miyamoto, MD, PhD; Tomohide Yoshino, MD; Atsushi Taniguchi, MD; Nobu Naiki, MD; Yoshihisa Sugimoto, MD, PhD; Makoto Ito, MD, PhD; Joel Q. Xue, PhD; Yoshitaka Murakami, PhD; Minoru Horie, MD, PhD

Background: Progressive cardiac conduction disease (PCCD), characterized by temporal increase in PR interval and QRS duration, may be attributed to diverse pathophysiological mechanisms. This study aimed to investigate whether PCCD is associated with increased risk of cardiovascular morbidity and mortality.

Methods and Results: Digital analysis of 12-lead ECG was performed to select patients with PCCD from among a database containing 359,737 ECGs. Long-term prognosis of PCCD was assessed in a large hospital-based population: 458 patients (341 males; mean age, 57.9±14.7 years) with PCCD were enrolled. During a mean follow-up of 13.3±6.4 years, 109 patients were hospitalized for heart failure (HF), and there were 16 and 59 deaths from cardiovascular diseases and all causes, respectively. Multivariate Cox proportional hazards analysis confirmed (1) a significant association of temporal incremental rate of PR interval (≥2 ms/year) and QRS duration (≥3 ms/year) with HF hospitalization (hazard ratio [HR], 2.34; 95% confidence interval [CI], 1.36–4.05; P=0.002 and HR, 2.08; 95% CI, 1.25–3.53; P=0.01, respectively) and (2) a significant association of temporal incremental rate of PR interval (≥4 ms/year) and QRS duration (≥5 ms/year) with cardiovascular mortality (HR, 6.9; 95% CI, 1.47–36.96; P=0.02 and HR, 4.31; 95% CI, 1.19–16.5; P=0.03, respectively).

Conclusions: The severity of PCCD was independently and significantly associated with HF hospitalization and cardiovascular mortality. (*Circ J* 2013; **77:** 60–67)

Key Words: Conduction; Electrocardiography; Heart failure; Prognosis; Ventricles

Progressive cardiac conduction disease (PCCD) is characterized by electrical deterioration of the conduction system in the atrium and ventricle, thus presenting as temporal prolongation of the PR interval and QRS duration. Lev and Unger[1] and Lenègre[2] reported pathological abnormalities in the conduction system with deposition of fibrous tissue in patients who developed ventricular conduction disturbance. On the other hand, inherited arrhythmias, including sick sinus syndrome, atrioventricular block and bundle branch block, have been reported. Several genetic abnormalities have been found in patients with inherited cardiac conduction abnormalities,[3] but although these disorders exhibit remarkable clinical characteristics such as syncope, sudden death and pacemaker implantation requirement, the prevalence is rare.

Editorial p41

In contrast, the relation of QRS duration with an increased rate of mortality[4,5] and reduced left ventricular ejection function[6] has been studied in numerous patients with and without ischemic heart diseases. In patients with myocardial infarction and reduced cardiac function, the benefit from implantable-cardioverter defibrillator therapy is higher when the QRS duration is longer.[7] These findings suggest that PCCD plays an important role in determining the prognosis of various cardiac disorders, including ischemic and nonischemic heart diseases.

However, little is known about the effect of temporal deterioration of supra- and intraventricular conduction on prognosis in a large hospital-based population. In Shiga University of Medical Science's hospital, more than 350,000 ECGs obtained from more than 100,000 patients are available for digital analysis. The long-term outcomes are precisely identified by the medical records. Using this large database, we systematically examined the association of PCCD with cardiovascular morbidity and mortality. This study also benefited from reproducible ECG measures based on computer-processed analyses.

Received July 2, 2012; revised manuscript received August 3, 2012; accepted August 23, 2012; released online September 26, 2012 Time for primary review: 8 days

Department of Cardiovascular and Respiratory Medicine (T.K., H.H., A.M., T.Y., A.T., N.N., Y.S., M.I., M.H.), Department of Medical Statistics (Y.M.), Shiga University of Medical Science, Otsu, Japan; and General Electric Healthcare, Milwaukee, WI (J.Q.X.), USA

Mailing address: Hideki Hayashi, MD, PhD, Department of Cardiovascular and Respiratory Medicine, Shiga University of Medical Science, Otsu 520-2192, Japan. E-mail: hayashih@belle.shiga-med.ac.jp

ISSN-1346-9843 doi:10.1253/circj.CJ-12-0849

Methods

The research protocol was approved by the Ethical Committee of Shiga University of Medical Science.

Study Population

In the University's hospital, digital recording of 12-lead ECGs started in January 1983. Until July 2010, a total of 114,334 consecutive patients (55,091 females and 59,243 males) underwent 12-lead ECG recordings in the supine position. The ECG database comprises a total of 359,737 ECGs collected during that period. The 12-lead ECG was recorded at rest for 10 s at a sweep speed of 25 mm/s, calibrated to 1 mV/cm in the standard leads. The data were digitally stored in a 12-bit server computer with a sampling interval of 2 ms.

From the database, we chose patients who exhibited wide QRS duration ≥120 ms between January 2000 and December 2003, enrolled in this study with the last follow-up on December 2010. To determine the temporal increase in QRS duration, the time interval of serial ECG recordings was at least ≥1 year. ECGs exhibiting Wolff-Parkinson-White syndrome, ventricular pacing, junctional or idioventricular rhythm and ventricular tachyarrhythmias were excluded. Patients who were <15 years old were also excluded from the analysis.

ECG Analysis

The ECG analysis was performed using software (MUSE7.1, GE Marquette Medical Systems, Inc, Milwaukee, WI, USA). Standardized, computerized ECG criteria as described by a 12-lead ECG analysis program were used to diagnose abnormal intraventricular morphologies. ECG variables, including duration, interval, amplitude, and axis, were digitally measured. For the ECG measurement, a median complex was computed as follows: (1) all QRS complexes of the same morphology were aligned in time and (2) the algorithm generated a representative QRS complex from the median voltages that were found at each successive sample time. QRS duration was measured from the earliest detection of depolarization in any lead (QRS onset) to the latest detection of depolarization in any lead (QRS offset). PR interval was measured in a similar manner. Because all variables of the 12-lead ECG were digitally measured based on computer-processed analysis, neither intra- nor interobserver variability needed to be taken into account and all measures were reproducible.

Follow-up

The follow-up period of all patients started from the day of the first ECG recording. We explored the prognostic factors for the endpoints of this study: cardiovascular death, all-cause death, and heart failure (HF) hospitalization. The outcome was assessed by searching the medical records in the hospital database. The determination of HF hospitalization was based on review of the hospital records. HF hospitalization had to satisfy both of the following criteria: (1) admission to hospital for ≥24 h with a clinical history of worsening symptoms of HF as evidenced by clinical criteria, including increased New York Heart Association functional class, orthopnea, paroxysmal nocturnal dyspnea, edema, exertional dyspnea, or gastrointestinal symptoms attributable to HF, and (2) one or more intensive treatments for HF within 24 h of admission, such as intravenous diuretics or inotropic agents. All ECGs taken during the follow-up were evaluated in patients enrolled in this study. The first ECG recording was assigned as the baseline ECG. The ECG recording in which the QRS duration was longest during follow-up was defined as the follow-up ECG.

Table 1. Baseline Demographics of the Patients

Total patients, n	458
Age (years)	57.9±14.7
Sex, male (%)	341 (74.5)
Follow-up period of ECG (years)	9.0±5.7
Survival period (years)	13.3±6.4
HF, n (%)	42 (9.2)
Ischemic heart disease, n (%)	55 (12.0)
Cardiomyopathy, n (%)	14 (3.1)
Hypertension, n (%)	160 (34.9)
Diabetes mellitus, n (%)	96 (21.0)
Valvular heart disease, n (%)	19 (4.1)
AF, n (%)	29 (6.3)
Arrhythmias*, n (%)	30 (6.6)
Malignant disease, n (%)	32 (7.0)
Cardiovascular surgery, n (%)	38 (8.3)
Other†, n (%)	31 (6.8)

Data are presented as mean±standard deviation and n (%).
*Arrhythmia involves patients with various types of rhythm disorder except for patients who exhibited AF when the ECG was recorded.
†Includes patients who suffered various internal diseases.
HF, heart failure; AF, atrial fibrillation.

Statistical Analysis

We described continuous variables using mean and standard deviation, and categorical variables using number and percentage. Comparisons between groups were made by t-test for continuous variables and χ^2 test for categorical variables. A receiver-operating characteristic curve was used to determine the cutoff point of prognostic factors that optimized the sensitivity and specificity of ECG variables for the endpoints. A Kaplan-Meier curve was created to describe the event-free survival rate and differences between groups were compared by log-rank test. Cox proportional hazards models were used to estimate hazard ratios of HF hospitalization, cardiovascular mortality and all-cause mortality adjusted by age, sex, and other confounding factors. Variables included in the Cox model were selected by a variable procedure with a criteria of $P<0.1$ for exclusion. All tests were 2-tailed and the significance level was set at 0.05. Because this study primarily evaluated cardiac conduction, we repeated the statistical analyses with patients without nodal-blocking agents such as β-blockers, Vaughan-Williams classes I, III, and IV anti-arrhythmic drugs, digitalis, and H2 histamine-blocker.

Results

A total of 458 consecutive patients (341 men; mean age, 57.9±14.7 years) were enrolled in this study. Among them, 109 (23.8%) were hospitalized because of HF. In addition, 59 (12.9%) patients died, of which cardiovascular death occurred in 16 (3.5%) patients. The mean duration of follow-up was 13.3±6.4 years.

Clinical Characteristics of the Patients

Table 1 shows the baseline clinical characteristics of the patients enrolled in this study. The study population consisted of patients with various cardiac diseases and other disorders including diabetes, malignancy, and surgery. The number of ECG recordings averaged 17.8±21 (median: 11) per patient. **Table 2** shows 12-lead ECG measures and morphological characteris-

Table 2. Characteristics of 12-Lead ECGs

	First ECG	Follow-up ECG	Temporal change*	P value
ECG measures				
Heart rate (beats/min)	68.6±14.1	66.1±13.1	−2.7±15.5	0.01
PR interval (ms)	165.0±27.4	178.5±34.0	13.9±20.2	<0.0001
QRS duration (ms)	118.9±22.8	142.9±15.4	24.0±22.5	<0.0001
QRS morphology				
Normal (n, %)	143, 31.2	0, 0	−31.2	<0.0001
RBBB (n, %)	186, 40.6	297, 64.8	24.2	<0.0001
RBBB with LAH (n, %)	13, 2.8	37, 8.1	5.3	0.0004
LBBB (n, %)	31, 6.8	47, 10.3	3.5	0.06
NSIVCD (n, %)	85, 18.6	76, 16.6	−2.0	0.43

Data are presented as mean±standard deviation and n (%).
*Temporal change indicates the difference in ECG measures or the prevalence of QRS morphology between the baseline ECG and the follow-up ECG.
RBBB, right bundle branch block; LAH, left anterior hemiblock; LBBB, left bundle branch block; NSIVCD, nonspecific intraventricular conduction disturbance.

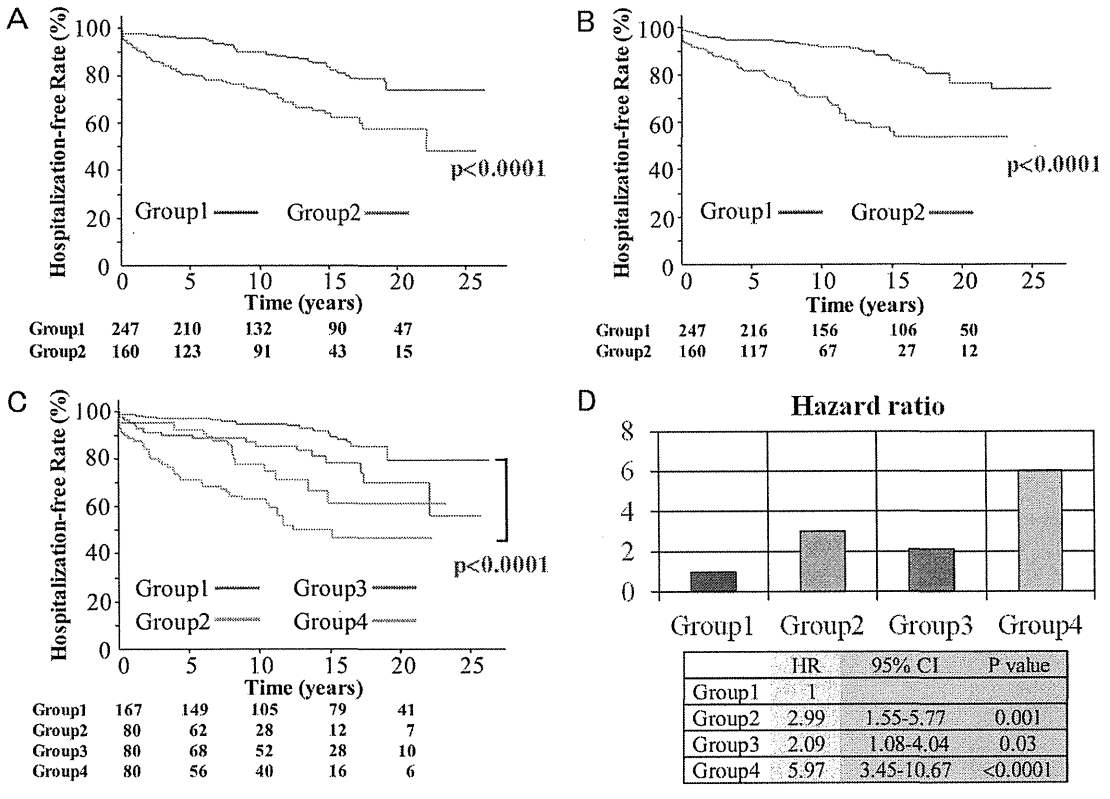

Figure 1. Kaplan-Meier survival analysis for a hospitalization for heart failure. (A) Temporal incremental rate of QRS duration <3ms/year (Group 1) vs. ≥3ms/year (Group 2). (B) Temporal incremental rate of PR interval <2ms/year (Group 1) vs. ≥2ms/year (Group 2). (C) Classification into 4 groups based on temporal incremental rate of QRS duration and PR interval: Group 1 consists of patients with QRS-duration incremental rate <3ms/year and PR-interval incremental rate of <2ms/year; Group 2, patients with QRS-duration incremental rate <3ms/year and PR-interval incremental rate ≥2ms/year; Group 3, QRS-duration incremental rate ≥3ms/year and PR-interval incremental rate <2ms/year; and Group 4, QRS-duration incremental rate ≥3ms/year and PR-interval incremental rate ≥2ms/year. (D) Interaction of hazard ratio of groups. Grouping is as in Panel C. Numbers of subjects at risk are shown under each graph.

Table 3. Univariate and Multivariate Survival Analyses of HF Hospitalization

	Univariate analysis (n=407)		Multivariate analysis (n=407)*		Multivariate analysis except nodal-blocking drugs (n=337)†	
	P value	HR (95% CI)	P value	HR (95% CI)	P value	HR (95% CI)
Age (<61 years=1)	0.04	1.55 (1.02–2.36)	0.18	1.37 (0.86–2.20)	0.16	1.47 (0.86–2.55)
Sex (female=1)	0.19	1.38 (0.86–2.33)	0.67	1.12 (0.67–1.95)	0.30	1.37 (0.76–2.57)
Heart rate (<66 beats/min=1)	0.21	1.30 (0.86–1.97)	0.26	1.29 (0.83–2.01)	0.29	1.34 (0.88–2.08)
Incremental rate of QRS duration (<3 ms/year=1)	<0.0001	2.52 (1.66–3.87)	0.01	1.79 (1.15–2.80)	0.01	2.08 (1.25–3.53)
Incremental rate of PR interval (<2 ms/year=1)	<0.0001	3.39 (2.22–5.23)	0.001	2.25 (1.42–3.58)	0.002	2.34 (1.36–4.05)

*Adjusted for age, sex, heart rate, arrhythmia except AF, nodal-blocking drugs, incremental rate of QRS duration, incremental rate of PR interval, diabetes mellitus, ischemic heart disease, and cardiomyopathy.
†Adjusted for age and sex, heart rate, arrhythmia except AF, incremental rate of QRS duration, incremental rate of PR interval, diabetes mellitus, ischemic heart disease, and cardiomyopathy.
HR, hazard ratio; CI, confidence interval. Other abbreviations as in Table 1.

tics of the QRS complex in the baseline and follow-up ECGs. Heart rate was significantly slower in the follow-up ECG than in the baseline ECG. PR interval and QRS duration significantly increased by 8.4% and 20.2%, respectively, during follow-up. In the baseline ECG, normal QRS duration was present in 31.2% of the study population, and right bundle branch block (RBBB), RBBB with left anterior hemiblock (LAH), left bundle branch block (LBBB), or nonspecific intraventricular conduction disturbance (NSIVCD) was present in the remaining patients. During the follow-up, RBBB, RBBB with LAH, and LBBB developed in 99 (21.6%), 9 (2.0%), and 22 (4.8%), respectively, of the patients who showed normal QRS duration in the baseline ECG. The prevalence of RBBB with or without LAH was significantly higher in the follow-up ECG than in the baseline ECG. The prevalence of LBBB showed a trend to increase during the follow-up, but the prevalence of NSIVCD did not significantly alter.

Long-Term Prognosis

HF The most common cause of the endpoints was HF hospitalization. During the follow-up period, 109 patients were hospitalized because of HF. At baseline, age was significantly higher in patients with HF hospitalization than in those without (60.7±11.2 vs. 57.0±15.5 years; P=0.02), but the sex prevalence was not significantly different between the 2 groups (76% vs. 74% male; P=0.64). The prevalence of ischemic heart disease, cardiomyopathy, valvular heart disease, and various arrhythmias excluding atrial fibrillation (AF) was significantly higher in patients with HF hospitalization than in those without (P<0.05 for each). The prevalence of diabetes and AF was marginally higher in patients with HF hospitalization than in those without (P=0.10 and 0.08, respectively). The follow-up period was not significantly different between patients with and without HF hospitalization (13.8±6.2 vs. 13.2±6.5 years, P=0.37). **Table S1** shows the ECG characteristics. In the baseline ECG, heart rate was significantly faster and QRS duration significantly shorter in patients with HF hospitalization than in those without, but the PR interval did not differ between patients with and without HF hospitalization. The prevalence of LBBB tended to be higher in patients with HF hospitalization than in those without, whereas for RBBB it was the reverse. The temporal increase in PR interval was significantly longer and the incremental rate of the PR interval was significantly higher in patients with HF hospitalization than in those without. The temporal increase in QRS duration was significantly longer and the incremental rate of QRS duration was significantly higher in patients with HF hospitalization than in those without.

Of the total patients enrolled, 43 and 8, respectively, developed AF and second- or third-degree atrioventricular block during the follow-up, and the PR interval failed to be measured in them, so they were excluded when the long-term prognosis was evaluated. Therefore, the final study sample in this analysis consisted of 407 patients (men, 300 [73.7%]; mean age, 57.4±15.1 years). **Figure 1** shows the Kaplan-Meier estimates of the probability of freedom from HF hospitalization. The temporal incremental rate of QRS duration of 3 ms/year or greater was associated with a significantly increased risk of HF hospitalization than that of <3 ms/year (hazard ratio [HR], 2.5; 95% confidence interval [CI], 1.66–3.87; P<0.0001) (**Figure 1A**). The temporal incremental rate of PR interval of 2 ms/year or greater was associated with a significantly increased risk of HF hospitalization than that of <2 ms/year (HR, 3.4; 95% CI, 2.22–5.23; P<0.0001) (**Figure 1B**). Furthermore, when present together, the temporal incremental rate of QRS duration and PR interval potentiated each other, leading to much higher rate of hospitalization for HF (HR, 6.0; 95% CI, 3.45–10.67; P<0.0001) (**Figure 1C**). **Table 3** shows the univariate and multivariate analyses in association with HF hospitalization. The temporal incremental rate of QRS duration and PR interval was significantly associated with HF hospitalization, even after exclusion of nodal-blocking drugs. Both ECG variables were independent of age, sex, and heart rate. Confounding diseases were not associated with HF hospitalization.

Cardiovascular Mortality A total of 16 patients died of cardiovascular causes during the follow-up: 12 from HF, 2 from ventricular tachyarrhythmia, 1 from cerebral hemorrhage, and 1 from occlusion of the celiac artery. At baseline, age was not significantly different between patients with and without cardiovascular death (63.3±11.8 vs. 57.7±14.7 years; P=0.14), nor was the sex prevalence between the 2 groups (88 vs. 74% male; P=0.19). The prevalence of cardiomyopathy was significantly higher in patients with cardiovascular death than in those without (18.8 vs. 2.5%; P=0.01), but the prevalence of ischemic heart disease, valvular heart disease, AF, and diabetes was not significantly different between the 2 groups. The prevalence of various arrhythmias excluding AF was marginally higher in patients with cardiovascular death than in those without (P=0.09). The follow-up period was not significantly different between patients with and without cardiovascular death (10.9±4.9 vs. 13.4±6.4 years, P=0.13). **Table S2** shows